ATMOSPHERIC ENVIRONMENT: X 5 (2020) 100059

Contents lists available at ScienceDirect

Atmospheric Environment: X

journal homepage: http://www.journals.elsevier.com/atmospheric-environment-x

Dual ground-based MAX-DOAS observations in Vienna, Austria: Evaluation of horizontal and temporal NO_2, HCHO, and CHOCHO distributions and comparison with independent data sets

Stefan F. Schreier[a,*], Andreas Richter[b], Enno Peters[b,1], Mareike Ostendorf[b], Alois W. Schmalwieser[c], Philipp Weihs[a], John P. Burrows[b]

[a] Institute of Meteorology and Climatology, University of Natural Resources and Life Sciences, Vienna, Austria
[b] Institute of Environmental Physics, University of Bremen, Germany
[c] Unit of Molecular Physiology and Biophysics, University of Veterinary Medicine, Vienna, Austria

ARTICLE INFO

Keywords:
MAX-DOAS
Nitrogen dioxide
Formaldehyde
Glyoxal
Urban pollution
Vienna

ABSTRACT

We characterize two recently installed MAX-DOAS instruments in Vienna, Austria, and evaluate horizontal path-averaged near-surface nitrogen dioxide (NO_2), formaldehyde (HCHO), and glyoxal (CHOCHO) volume mixing ratios (VMRs) over the urban area by applying a state-of-the-art retrieval approach. As Vienna is influenced by Pannonian continental climate, characterized by hot summers and cold winters, a temperature correction is introduced and applied to the NO_2 differential slant column densities (DSCDs) retrieved in the visible spectral range to correct for the temperature dependence of the NO_2 cross-section. The results show that not accounting for such a correction leads to an overestimation of absolute values by up to 15% in the winter season. Path-averaged NO_2 VMRs from selected horizontal viewing directions are compared with surface NO_2 VMRs from air quality monitoring stations located below and/or in close proximity to the particular MAX-DOAS line of sight. Good agreement between the two independent data sets is found, in particular during the summer season, with correlation coefficents ranging between 0.76 and 0.94. Seasonal and diurnal cycles of path-averaged NO_2, HCHO, and CHOCHO VMRs are evaluated for a full year of measurements taken at the lowest elevation angles. While the highest daytime monthly averages of NO_2 VMRs are found in winter, peaks of HCHO occur in summer. Highest amounts of CHOCHO conversely are observed over the course of the year, with the exception of summer. Seasonally-averaged diurnal cycles indicate that elevated NO_2 and CHOCHO amounts are generally found in the morning hours and that there is a clear difference in trace gas amounts between weekdays and weekends when pointing at anthropogenic sources. The horizontal variabilty of tropospheric NO_2, HCHO, and CHOCHO amounts is investigated by analyzing seasonally-averaged path-averaged VMRs, again obtained from measurements taken at the lowest elevation angles. The results show that highest amounts of NO_2 and CHOCHO are found when the MAX-DOAS instruments are pointing towards the city center and/or towards busy roads and industrial areas, whereas highest amounts of HCHO are found over northern and western parts of Vienna, in particular in summer, which implies that anthropogenic sources are not the dominant drivers of HCHO production during that time of the year. Finally, the influence of wind direction and wind speed on tropospheric NO_2, HCHO, and CHOCHO amounts is evaluted. The results show that tropospheric pollution levels over the city center of Vienna are highest at low wind speeds and wind directions from the Southeast.

1. Introduction

Nitrogen dioxide (NO_2), one of the most important trace gases in the atmosphere, plays a key role in both tropospheric and stratospheric chemistry (Crutzen, 1979). In the troposphere, it is a crucial air pollutant because of its participation in catalytic cycles that lead to the formation of ozone (Crutzen, 1970) and due to its precursor role for secondary organic aerosols (Jang and Kamens, 2001). The oxidation of NO_2 can

* Corresponding author.
E-mail address: stefan.schreier@boku.ac.at (S.F. Schreier).
[1] Now at: Institute for the Protection of Maritime Infrastructures, German Aerospace Center (DLR), Bremerhaven, Germany.

https://doi.org/10.1016/j.aeaoa.2019.100059
Received 26 April 2019; Received in revised form 21 November 2019; Accepted 22 November 2019
Available online 26 November 2019
2590-1621/© 2019 The Authors. Published by Elsevier Ltd. This is an open access article under the CC BY license (http://creativecommons.org/licenses/by/4.0/).

lead to the formation of nitric acids, which are deposited afterwards either in precipitation or in dry form (Finlayson-Pitts and Pitts, 2000). Anthropogenic and natural sources of nitrogen oxides ($NO_x = NO + NO_2$) include fossil fuel combustion, biomass burning, lightning, and soil emissions (Delmas et al., 1997). In urban environments, NO_x are dominantly emitted by combustion processes in vehicle traffic, power generation, and industry. As the residence time of NO_x is relatively short in the lower troposphere (i.e. a few hours), NO_2 is usually found close to its sources, in particular during calm wind conditions (Beirle et al., 2011).

Formaldeyde (HCHO) is a short-lived oxidation product of volatile organic compounds (VOCs) and hydrocarbons, including methane (CH_4). The degradation of the latter trace gas is a well-mixed source of HCHO determining its global background concentrations (Singh et al., 2001). The variability of tropospheric HCHO amounts over land surfaces results from the oxidation of biogenic, pyrogenic, and anthropogenic non-methane VOCs (NMVOCs). In addition to the production from NMVOC oxydation, HCHO can also be directly emitted from biomass burning, vegetation, and fossil fuel combustion. It is estimated, that over urban environments, primary emissions and secondary production of HCHO account for about 5% and 95%, respectively (Palmer et al., 2003; Fu et al., 2007; De Smedt et al., 2010; Parrish et al., 2012). For example, VOCs and their degradation products affect the formation of tropospheric ozone (e.g., Houweling et al., 1998). Due to its short lifetime, HCHO is often used as a tracer for non-methane VOC emissions.

Another short-lived product of atmospheric oxidation of VOCs is glyoxal (CHOCHO). Although primary emissions of CHOCHO are presumed to be rather small, secondary production from the oxidation of VOCs emitted by the biosphere can lead to high concentrations over areas with large biogenic emissions (e.g. from oxydation of alkenes and aromatic species) and over areas associated with biomass burning (Wittrock et al., 2006; Stavrakou et al., 2009; Vrekoussis et al., 2009; Lerot et al., 2010; Alvarado et al., 2014; Chan Miller et al., 2014). Additionally, high glyoxal amounts have also been found over polluted environments. Such elevated amounts result from the combination of VOCs emitted from both anthropogenic and biogenic emission sources (e.g. Volkamer et al., 2005a). In addition to a variety of other removal processes (e.g. reaction with OH), the dominant sink of CHOCHO is photolysis (Fu et al., 2008).

Because of their distinct electronic vibrational absorption structures in the ultraviolet (UV) and visible (Vis) region of the electromagnetic spectrum, NO_2, HCHO, and CHOCHO can be measured with the Differential Optical Absorption Spectroscopy (DOAS) method, first described by Perner and Platt (1979). Originally, DOAS was applied to measure tropospheric trace gases (e.g. NO_2) by using artificial light sources (active DOAS). A few years later, DOAS was also applied to direct and scattered sunlight obseravtions (passive DOAS). The passive DOAS approach was initially used to observe stratospheric trace gas amounts by pointing the telescope into the zenith direction. The main difference between the active and passive DOAS methods lies in the knowledge of the light path length. While it is clearly defined for active DOAS, efforts are needed to determine the effective light path length in the atmosphere for passive DOAS. The passive DOAS principle has been applied to various ground-based, ship-based, aircraft-based, and satellite-based platforms (e.g. Burrows et al., 1995, Burrows et al., 1999, Platt and Stutz, 2008 and references therein; Burrows et al., 2011 and references therein).

After successful application of the zenith scattered light DOAS, which mainly yields stratospheric trace gas amounts (e.g. Noxon, 1975; Solomon et al., 1987; Richter et al., 1999; Wittrock et al., 2000), the development of Multi-AXis (MAX) DOAS allowed for the extension of this technique to tropospheric trace gases and aerosols by observing scattered sunlight at different elevation angles (Hönninger et al., 2004; Wagner et al., 2004; Wittrock et al., 2004). The trace gas concentration integrated along the effective light path or slant column density (SCD) is determined by applying the DOAS method. To be more specific, the result of the spectral fit is the difference in slant column amounts of specific absorbers (e.g. NO_2, HCHO, and CHOCHO) between the measurement and the reference, often called "Differential Slant Column Density" (DSCD).

Past studies have shown the potential to derive NO_2, HCHO, and CHOCHO tropospheric columns in urban environments from one MAX-DOAS instrument having a particular scanning geometry (e.g. Kramer et al., 2008; Wagner et al., 2011; Ma et al., 2013; Hendrick et al., 2014; Vlemmix et al., 2015; Gratsea et al., 2016; Wang et al., 2017; Xing et al., 2017; Chan et al., 2018). In most of the mentioned studies, the obtained DSCDs were converted into tropospheric vertical columns.

Recently, an approach for the conversion of MAX-DOAS DSCDs into near-surface box-averaged mixing ratios was introduced (Sinreich et al., 2013). The approach focuses on measurements taken at low elevation angles, e.g. where the sensitivity is highest, and weakly depends on aerosol layer height. The calculation of the effective light path length (L) is based on O_4 DSCDs, and thus systematic errors can be introduced by the method when the vertical profile of the trace gas differs from that of O_4. In order to reduce these errors, correction factors have been computed with radiative transfer models (Sinreich et al., 2013; Wang et al., 2014). In cases where the MAX-DOAS instrument is located above the aerosol layer (e.g. on top of a mountain) and by making the assumption that the last scattering event is close to the altitude of the instrument, the use of these correction factors is not needed and the method is then based on geometry only (Gomez et al., 2014; Schreier et al., 2016). More recently, the (geometrical) approach has been applied without using correction factors for MAX-DOAS measurements taken from towers at a coastal site near Hamburg as well as in the urban environment of Vienna (Seyler et al., 2017; Schreier et al., 2019).

The motivation of the VINDOBONA (VIenna horizontal aNd vertical Distribution OBservations Of Nitrogen dioxide and Aerosols) project (http://www.doas-vindobona.at/), which is financed by the Austrian Science Fund (FWF) and the German Research Foundation (DFG), was the existence of two infrastructures with ideal measurement conditions in Vienna, enabling long-term MAX-DOAS observations. Such measurements serve as basis for improvements of NO_2 and aerosol retrievals where the sensitivity is expected to be rather high – in a large city.

Vienna is the capital and largest city of Austria with a population in excess of 1.8 million (2.8 million including the population in the surrounding areas). The urban agglomeration of Vienna and the surrounding area is located in northeastern Austria in the Vienna basin and close to the easternmost extension of the Alps. Since the number of inhabitants in and around Vienna is expected to further increase during the next years to reach 2 million by the year 2025 (https://www.statistik.at/), Austria's largest city can be seen as a typical example of a growing city.

The overaching goal of the VINDOBONA project is to improve our current knowledge of man-made air pollution in urban environments. The main emphasis is placed on the installation and operation of two MAX-DOAS instruments, the characterization of the horizontal, vertical, and temporal variations of tropospheric trace gases and aerosols, the improvement of tropospheric trace gas and aerosol retrievals, and the validation of trace gas columns retrieved from satellite instruments.

The focus of this paper is on (i) the characterization of the two MAX-DOAS instruments, (ii) the analysis of path-averaged near-surface NO_2, HCHO, and CHOCHO VMRs in the horizontal viewing direction obtained from the first year of measurements, and (iii) the comparison of retrieved path-averaged NO_2 VMRs with surface NO_2 VMRs as obtained from the existing network of air quality monitoring stations in Vienna.

2. Measurements and methodology

2.1. MAX-DOAS measurements

2.1.1. VETMED instrument

The first of the two MAX-DOAS instrument, which is located on the campus of the VETerinärMEDizinische (VETMED) Universität Wien (48° 15′ 26.45″ N, 16° 25′ 54.4″ E, 171 m a.s.l.) (Fig. 1), comprises a spectrometer (Acton Standard Series SP-2356 Imaging Spectrograph), a charge-coupled device (CCD) detector (Princeton Instruments PIX100B-SF-Q-F-A), a telescope unit mounted on a pan/tilt head, optical fibres, cables, and a measuring computer. Both the spectrometer (+35 °C) and the detector (-55 °C) are temperature-controlled and placed inside the building. Due to many campus and apartment buildings in the immediate vicinity, the telescope unit was mounted on a 7 m high measuring mast that was installed on the roof of the building, leading to a total measuring height of 11 m above ground.

The VETMED Vis MAX-DOAS (hereafter referred to as VETMED instrument) performs spectral measurements between 399 and 533 nm, at a spectral resolution of 0.75 nm and with a field of view of ~0.8°. Typical integration times are 30 and 60 s in the off-axis and zenith-sky modes, respectively. While the azimuthal and elevation angle capabilities are fully configurable, direct-sun measurements are not possible with this measurement system.

Before the VETMED instrument was set up in December 2016 on the roof a VETMED campus building, it participated in the CINDI-2 (second Cabauw Intercomparison campaign for Nitrogen Dioxide measuring Instruments) campaign (Kreher et al., 2019).

Detector nonlinearity, pixel-to-pixel variability, and field of view were characterized in the IUP-Bremen laboratory and during the CINDI-2 campaign in summer and fall, respectively, of the year 2016. Other calibration and characterization procedures such as nightly measurements for dark signal and HgCd lamp measurements for line shape are performed on a routine basis.

2.1.2. BOKU instrument

The second of the two MAX-DOAS instruments was set up in April 2017 on the roof of Schwackhöferhaus at the Universität für BOdenKUltur (BOKU) Wien (48° 14′ 16.45″ N, 16° 19′ 54″ E, 267 m a.s.l.) (Fig. 1), which is about 7.75 km to the west of the VETMED site.

Overall, the BOKU UV MAX-DOAS instrument (hereafter referred to as BOKU instrument) is similar to the VETMED instrument with the exception of a different spectrometer (Shamrock SR-193i-A) and CCD detector (ANDOR IDUS DV420A-BU). Temperature control is also configured for the BOKU spectrometer (+35 °C) and detector (-35 °C), which are both also located inside the building. Because of its location on a hill, the BOKU instrument has an unblocked view towards the city center, in contrast to the VETMED instrument.

In contrast to the visible spectral range covered by the VETMED instrument, the BOKU instrument performs measurements in the ultraviolet range between 299 and 399 nm. Spectral resolution and field of view of the BOKU instrument are 0.5 nm and 0.8°, respectively. Integration times as well as azimuthal and elevation angle capabilities are the same as for the VETMED instrument and calibration/characterization procedures are also performed on a routine basis.

2.1.3. Selection of azimuthal viewing directions and elevation angles

A total of six azimuthal directions, including horizontal ligth paths that cover high-traffic roads, industrial zones, but also residential and rural areas, were selected for both instruments (Fig. 1). One azimuthal direction of each instrument was chosen to point towards the location of the other instrument (blue line) and another was chosen to point towards the city center (red line). The azimuth angles (AAs) of the selected viewing directions are (starting from North in a clockwise direction) 0° (cyan), 170° (green), 190° (yellow), 225° (red), 254° (blue), and 300° (magenta) for the VETMED and 74° (blue), 88° (green), 129° (yellow), 137° (red), 144° (cyan), and 213° (magenta) for the BOKU instrument. The azimuthal viewing directions of the VETMED instrument correspond to suburban and rural areas (0°), industrial zones including high-traffic roads (170° and 190°), the urban core (225°), and suburban/urban areas including high-traffic roads (254° and 300°), whereas the ones of the BOKU instrument correspond to suburban/urban areas including high-traffic roads (74° and 88°), the urban core (129°, 137°, and 144°), and suburban areas (213°). For all azimuthal viewing directions, a consistent elevation sequence with consecutive elevation angles (EAs) of 0°, 1°, 2°, 3°, 4°, 5°, 10°, 15°, 30°, and 90° is configured.

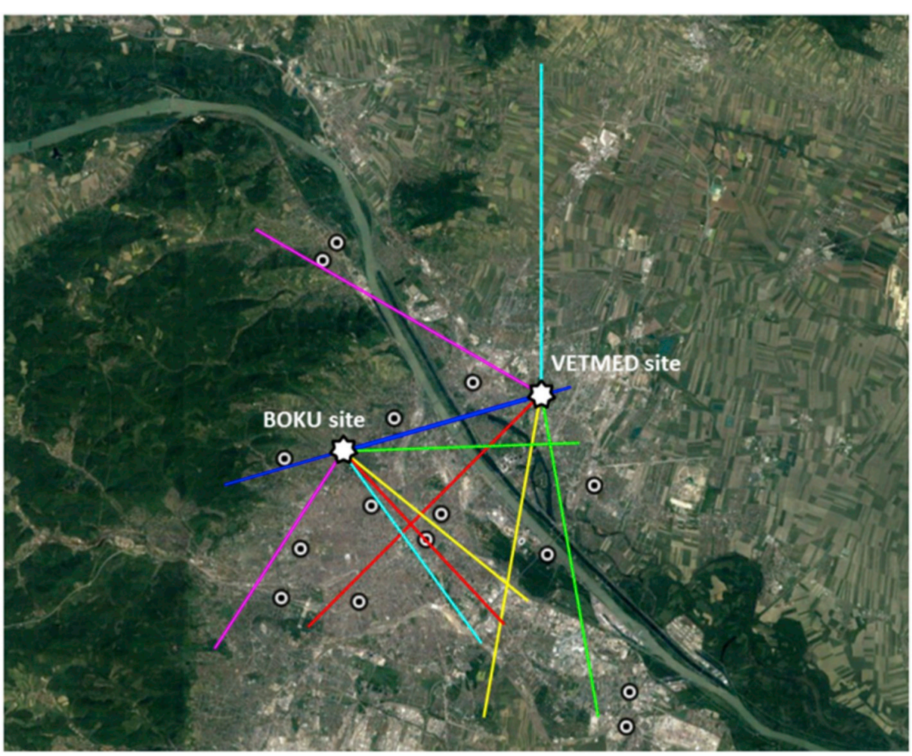

Fig. 1. Geographical location of the VETMED and BOKU MAX-DOAS instruments with their associated azimuthal viewing directions: 0° (cyan), 170° (green), 190° (yellow), 225° (red), 254° (blue), and 300° (magenta) (VETMED instrument) as well as 74° (blue), 88° (green), 129° (yellow), 137° (red), 144° (cyan), and 213° (magenta) (BOKU instrument). For schematic representation, the ground projected MAX-DOAS light paths, which are used for the selection of air quality monitoring stations for comparison (see Table 4), are set to 12.9 and 9.3 km for the Vis (VETMED) and UV (BOKU) instruments, following the results of Seyler et al. (2017). The circled dots display the geographical position of air quality monitoring stations, which are used for comparison in this study. (For interpretation of the references to color in this figure legend, the reader is referred to the Web version of this article.)

One elevation sequence at one azimuthal viewing direction lasts for about 6 min, resulting in about 36 min for one full azimuthal scan.

In order to test, whether the field of view for the lowest EAs of the selected AAs is blocked by any obstacles such as trees and/or houses, so-called skyline scans have been performed on 18 May 2017, which was a day with cloudless conditions. The scans were conducted with the VETMED and BOKU instruments in a clockwise direction with azimuthal angle steps of 1° for EA = 1°, 2°, and 3° and EA = 0°, 1°, and 2°, respectively. The measured intensity recorded at the different EAs and plotted as a function of AAs is shown in Fig. 2 for the VETMED (left panel) and BOKU (right panel) instruments. For an easier interpretation of the results, the selected azimuthal viewing directions of the two instruments are indicated by colored dots on the outermost circle of the graphs in the left and right panels of Fig. 2.

A large variability of intensity is found for the measurements taken at lowest elevation angles (EA = 1 and 2°) with the VETMED instrument, indicating that the vision is blocked at various azimuthal directions. This is because of the position of the MAX-DOAS instrument relative to sligthly higher campus buildings within the immediate vicinity. In contrast, a rather smooth curve is obtained for EA = 3° with this instrument, indicating that at this elevation, the buildings are not blocking the vision anymore (see Fig. 2, left panel). The BOKU instrument is mounted on a measurement platform on top of a campus building at an elevated location, which is almost 100 meteres higher than the city center. In addition to its favorable topographic position, there are only a few tall buildings that block the view of the instruments at EA = 1°. We overcome this by selecting azimuthal viewing directions that are pointing between such obstacles (Fig. 2, right panel).

In summary, we find that the lowest EAs, which are best suited for further analyses of the obtained NO_2, HCHO, and CHOCHO DSCD measurements, are 3° (VETMED instrument) and 1° (BOKU instrument).

2.1.4. DOAS analysis of NO_2, HCHO, and CHOCHO differential slant column densities (DSCDs)

The spectral measurements obtained from the two MAX-DOAS instruments are analyzed using the DOAS technique applying a nonlinear least-squares fitting algorithm (e.g. Platt and Stutz, 2008 and references therein) developed at IUP-UB (Richter, 1997).

For NO_2 and CHOCHO retrieved in the visible channel, spectral fitting windows from 425 to 490 nm and 433–458 nm were selected (Table 1), respectively, whereas spectral ranges of 338–370 nm and 336.5–359 nm were chosen for NO_2 and HCHO in the ultraviolet channel (Table 2), following the recommendations made during CINDI-2 (Kreher et al., 2019). The retrieval of differential slant column densities (DSCDs) uses zenith-sky measurements of the same elevation sequence as Fraunhofer reference spectrum. In addition to the above mentioned trace gases, O_4 DSCDs are also obtained from spectral fitting in the Vis and UV windows that are used to retrieve NO_2 DSCDs. More details on the spectral fitting in the visible and ultraviolet channels are listed in Tables 1 and 2, respectively.

Typical examples of fit results as obtained from measurements taken on 14 September 2017 are shown in Fig. 3. The two spectra were recorded at AA = 225°, EA = 3°, and SZA = 55.96° with the VETMED and at AA = 137°, EA = 1°, and SZA = 47.63° with the BOKU

Table 1
Parameter settings used in the visible (Vis) retrieval of NO_2, O_4, and CHOCHO DSCDs.

Fit parameter		Selection/Source
Spectral range		425–490 nm (NO_2, O_4) 433–458 nm (CHOCHO)
Polynomial (number of coefficients)		6 (NO_2) and 3 (CHOCHO)
Wavelength calibration		Solar atlas (Kurucz et al., 1984)
Fraunhofer reference		Sequential zenith spectrum
Cross section	**Temperature**	**Data source**
O_3	223 K	Serdyuchenko et al. (2014)
NO_2	298 K	Vandaele et al. (1996)
	220 K	Vandaele et al. (1996), orthogonalized
O_4	293 K	Thalman and Volkamer (2013)
CHOCHO	296 K	Volkamer et al. (2005b)
H_2O	296 K	Rothmann et al. (2003)
Ring	–	QDOAS

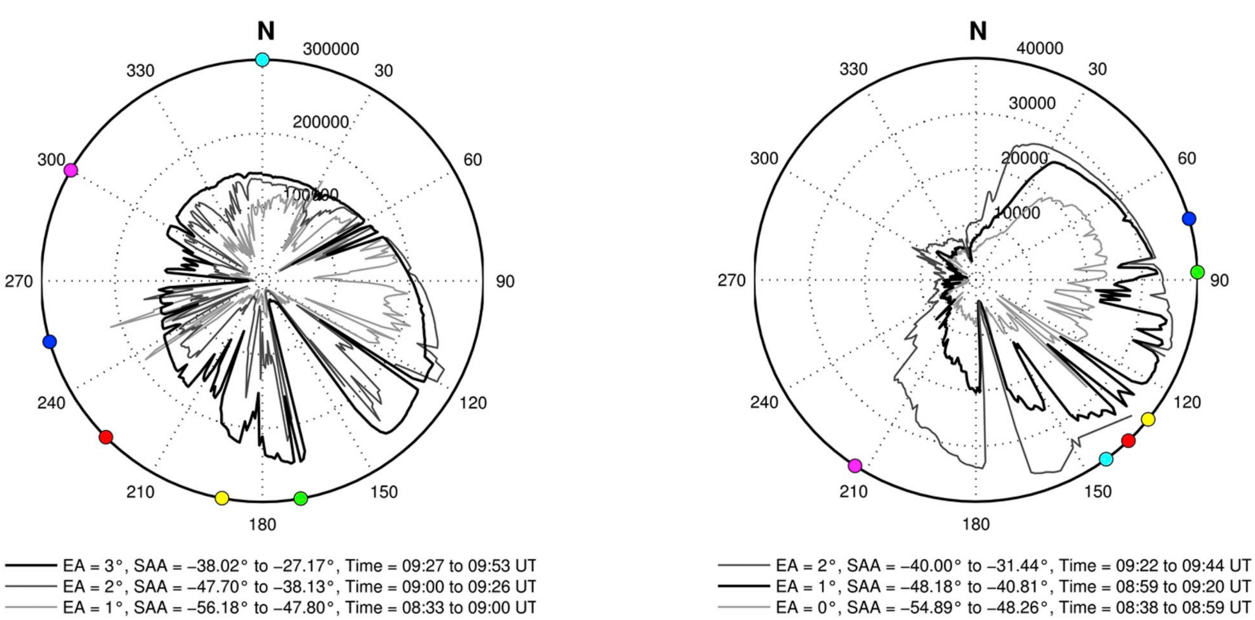

Fig. 2. Horizontal intensity scans performed with the VETMED (left) and BOKU (right) instruments in the morning of 18 May 2017 during cloudless conditions for azimuthal angle steps of 1° and for three different elevation angles. The black thick curves displayed in the two graphs represent the lowest elevation angles used for the analysis of spectral data in this study (EA = 3° for the VETMED and EA = 1° for the BOKU instrument). The blue, cyan, green, magenta, red, and yellow colored dots on the outermost circle of the graphs indicate the selected azimuthal viewing directions of the two instruments. The solar azimuthal angle (SSA) and time (UT) of the individual scans are given in the legend. (For interpretation of the references to color in this figure legend, the reader is referred to the Web version of this article.)

Table 2
Parameter settings used in the ultraviolet (UV) retrieval of NO_2, O_4, and HCHO DSCDs.

Fit parameter		Selection/Source
Spectral range		338–370 nm (NO_2, O_4) 336.5–359 nm (HCHO)
Polynomial degree (number of coefficients)		6
Wavelength calibration		Solar atlas (Kurucz et al., 1984)
Fraunhofer reference		Sequential zenith spectrum
Cross section	**Temperature**	**Data source**
O_3	223 K	Serdyuchenko et al. (2014)
	243 K	Serdyuchenko et al. (2014)
NO_2	298 K	Vandaele et al. (1996)
	220 K	Vandaele et al. (1996), orthogonalized
O_4	293 K	Thalman and Volkamer (2013)
HCHO	293 K	Meller and Moortgat (2000)
BrO	223 K	Fleischmann et al. (2004)
Ring	–	QDOAS

instrument.

In summary, the spectral fitting procedure delivers fits with overall good quality of the trace gas DSCDs for both instruments, in particular for NO_2, but also for HCHO and CHOCHO during those times of the year when increased amounts occur. For optimal measurement conditions (e.g. clear sky and elevated trace gas amounts), fit errors of retrieved DSCDs are <0.25% (NO_2 in the visible spectral range), <2% (NO_2 in the UV spectral range), <10% (HCHO), and <15% (CHOCHO).

2.1.5. Temperature correction of NO_2 DSCDs

Due to its geographical location in the mid-latitudes and the distance from large water bodies that could dampen air temperatures in summer and winter, the climate in Vienna is Pannonian continental with hot summers and cold winters. Current and archived weather data from the BOKU weather station can be found and downloaded at https://meteo.boku.ac.at/wetter/aktuell/.

The NO_2 absorption cross-section has a pronounced temperature dependence, both in the absolute value and in the differential structures. For optical remote sensing measurements of NO_2 amounts in the atmosphere, e.g. MAX-DOAS, this has to be taken into account for the visible spectral range, to improve the accuracy of the retrieved values.

Typical DOAS retrieval settings used to retrieve the NO_2 DSCDs in the visible spectral range consider as well as absorption cross-sections for other trace gases, two NO_2 absorption cross-sections – one evaluated at 220 K (accounting for NO_2 in the stratosphere) and one at 298 K (accounting for NO_2 in the troposphere) (e.g. Kreher et al., 2019). It is important to note here that about 25% and up to more than 90% of atmospheric NO_2 can reside in the stratosphere over polluted and unpolluted regions, respectively (Dirksen et al., 2011). During the bulk of the season, the effect of higher and/or in particular lower air temperatures in the lowermost boundary layer, e.g. where the horizontal MAX-DOAS measurements are taken, are considered to be negligibly small. For rather cold days in winter however, a NO_2 cross-section evaluated in the laboratory at room temperature might not be representative enough anymore.

In this study, where horizontal NO_2 DSCDs are analyzed for the whole season over a city where NO_2 pollution is an important issue, the

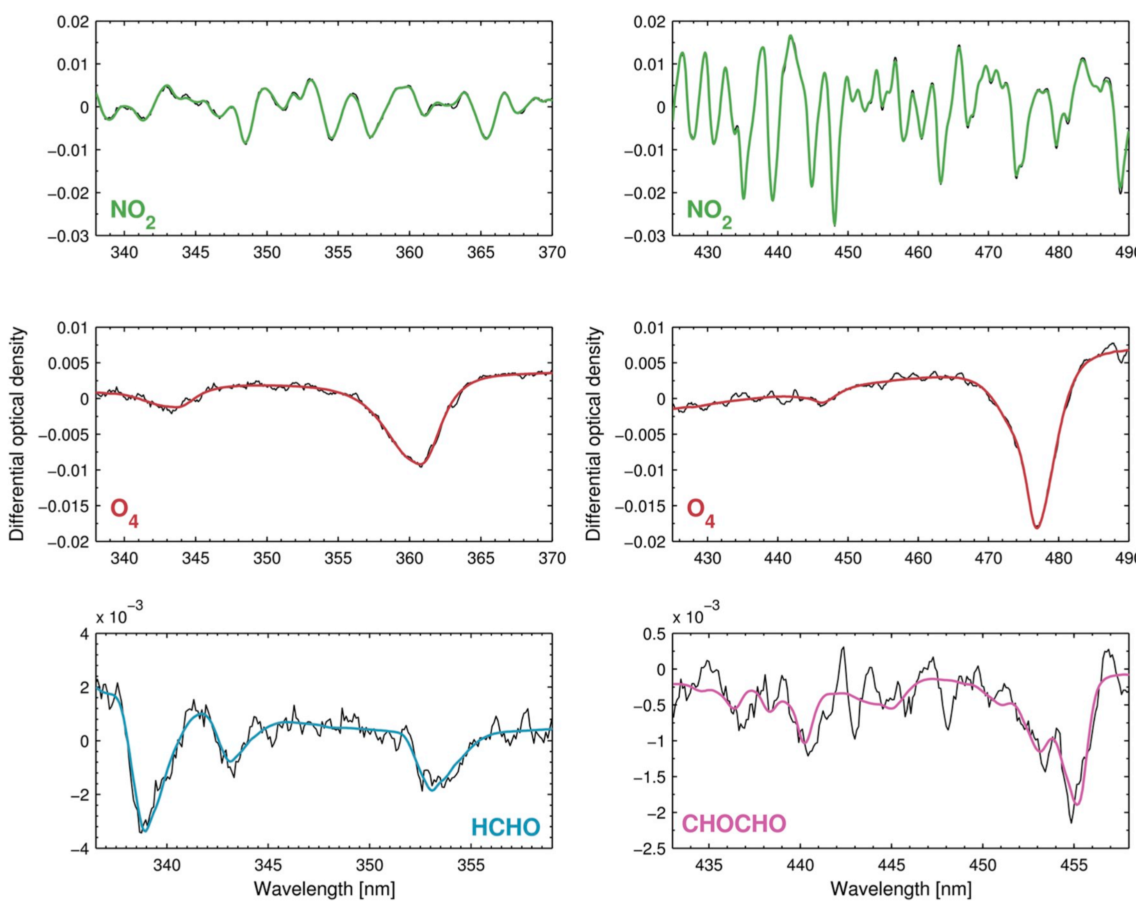

Fig. 3. Examples of NO_2, O_4, HCHO, and CHOCHO differential slant column fit results as obtained from the two MAX-DOAS instruments on 14 September 2017. The two spectra were recorded at AA = 137°, EA = 1°, SZA = 47.63° (BOKU UV instrument, left panels) and at AA = 225°, EA = 3°, SZA = 55.96° (VETMED Vis instrument, right panels).

temperature dependence of the NO_2 cross-section for spectral fitting in the visible range is compensated by introducing an empirical temperature correction:

$$DSCD_{corrected} = DSCD\ (NO_2\ @\ T_{ref}) * \{1.0 + (T_{surface} + (T_{surface} - (MH+27) / 1000*7)) / 2) * 0.00357\}, \quad (1)$$

where T_{ref} corresponds to the temperature at which the NO_2 absorption cross-section was evaluated in the laboratory (e.g. Vandaele et al., 1996) and $T_{surface}$ refers to the observed air temperature at 2 m above ground. In order to account for the vertical distribution of NO_2, which for reasons of simplicity is assumed to be uniformly distributed throughout the whole boundary layer, measured mixing-height (MH) as well as a lapse rate of 7°C per kilometer are introduced in Eq. (1). An offset of 27 m is added to the provided mixing-height data to account for the fact that the ceilometer instrument at the Austrian weather service is located 27 m above the location of the VETMED instrument. The values of $T_{surface}$ with a temporal resolution of 10 min are obtained from the ZAMG weather station, which is located on the same measurement platform as the ceilometer instrument. The scaling factor 0.00357 was determined from DOAS fits using NO_2 cross-sections at different temperatures.

2.1.6. *Conversion of NO_2, HCHO, and CHOCHO DSCDs into path-averaged near-surface VMRs*

We follow the conversion approach introduced by Sinreich et al. (2013) and estimate path-averaged near-surface VMRs of NO_2, HCHO, and CHOCHO as retrieved from measurements taken at the lowest elevation angles of the two MAX-DOAS instruments. In a first step, O_4 DSCD measurements are used for the estimation of the effective light path length (L):

$$L = DSCD_{(O4)} / n_{(O4)}, \quad (2)$$

where n_{O4} is the near-surface O_4 concentration, which is calculated by using air pressure and air temperature measurements from a nearby weather station (see Sect. 2.2.2):

$$n_{(O4)} = (n_{(O2)})^2 = (0.20942 * n_{(air)}), \quad (3)$$

$$n_{(air)} = (p_{surface} * N_A) / (T_{surface} * R), \quad (4)$$

where $n_{(air)}$ is the number density of air and $p_{surface}$ and $T_{surface}$ are the air pressure and air temperature at the surface level. N_A and R denote Avogadro's number and universal gas constant, respectively, and 0.20942 is the mixing ratio of oxygen. It is important to note that L is the difference between the light path lengths for the horizon measurements (EA = 3° for the VETMED and EA = 1° for BOKU instrument) and the Fraunhofer reference spectrum, which is taken in the zenith direction and close in time (<5 min) before and/or after the horizontal measurements are taken. In a second step, L is used for the conversion of trace gas DSCDs into path-averaged near-surface VMRs:

$$n_{(NO2,\ HCHO,\ CHOCHO)} = DSCD_{(NO2,\ HCHO,\ CHOHCO)} / L, \quad (5)$$

$$c_{(NO2,\ HCHO,\ CHOCHO)} = (n_{(NO2,\ HCHO,\ CHOCHO)} * M_i) / N_A, \quad (6)$$

$$X_{(NO2,\ HCHO,\ CHOCHO)} = c_{(NO2,\ HCHO,\ CHOCHO)} * (1 / M_i) * (R * T_{surface} / p_{surface}), \quad (7)$$

where $n_{(NO2,\ HCHO,\ CHOCHO)}$, $c_{(NO2,\ HCHO,\ CHOCHO)}$, and $X_{(NO2,\ HCHO,\ CHOCHO)}$ are the trace gas number density in units [molecules cm^{-2}], mass column densities in units [g cm^{-2}], and volume mixing ratio in units [ppb] respectively. M_i denotes the molar mass of trace gases.

Recent studies have introduced correction factors for reducing errors resulting from the conversion approach because of the difference in vertical profiles of O_4 and NO_2, HCHO, and CHOCHO (Sinreich et al., 2013; Wang et al., 2014). Here, we follow the argumentation of Seyler et al. (2017) and do not consider correction factors in our study. As we are focusing on measurements taken at EA = 3° (VETMED instrument) and EA = 1° (BOKU instrument), errors of the derived VMRs are expected to be low as correction factors are usually close to unity for such low elevation angles. Correction factors and expected errors in the conversion approach are discussed in detail in the above mentioned literature.

2.2. *Ancillary data*

2.2.1. *Surface in situ measurements of NO_2 concentrations*

One of the main focusses of this paper is the comparison of NO_2 mixing ratios obtained from measurements at the lowest viewing directions of the two MAX-DOAS instruments with NO_2 concentrations measured by ground-based air quality monitoring stations. The motivation behind this systematic comparison is to investigate whether MAX-DOAS data can deliver information, which is comparable to air quality monitoring data. The NO_2 surface concentrations used in this study are provided by the Vienna Municipal Department for Environmental Matters, the Provincial Government of Lower Austria, and the Environment Agency Austria (e.g. Spangl and Nagl, 2017).

Half-hour averages of NO_2 concentrations from a total of fifteen air quality monitoring stations within (twelve stations) and outside (three stations) the borders of Vienna are selected for this comparison purpose (Fig. 1 and Table 3). NO_2 concentrations are currently detected with Horiba APNA-370 and API M200E (NOx) instruments at these stations (Spangl and Nagl, 2017). The combined measurement uncertainty is about 10% for these instruments (W. Spangl, personal communication, 2018).

In order to make these data comparable in terms of units with path-averaged near-surface VMRs derived from measurements of the two MAX-DOAS instruments, mass concentrations are converted into VMRs in an analogous manner (see Eq. (7)).

2.2.2. *Ground-based meteorological measurements of air pressure, air temperature, global radiation, mixing-height, wind direction, and wind speed*

For the interpretation of trace gas distributions in the planetary boundary layer of the Viennese metropolitan area, meteorological measurements of air pressure ($p_{surface}$), air temperature ($T_{surface}$), global radiation, mixing-height, wind direction, and wind speed are used.

Measurements of $p_{surface}$, $T_{surface}$, wind direction, and wind speed with a temporal resolution of 10 min as well as 5-min averages of mixing-height (Lotteraner and Piringer, 2016) are provided by the Austrian weather service (ZAMG) for the station Hohe Warte (48° 14′ 55″ N, 16° 21′ 23″ E, 198 m a.s.l). The correction of NO_2 DSCDs (see Sect. 2.1.5) is based on $T_{surface}$ measurements from this station, which is located about 5.6 km from the location of the VETMED instrument. Meteorological data from the ZAMG weather station are also used for the computation of L from measurements taken with the VETMED instrument. Measurements of $p_{surface}$, $T_{surface}$ as well as global radiation with a temporal resolution of 10 min are provided by the BOKU weather station, which is at the same location as the BOKU instrument. The former two variables are used for the calculation of L from measurements taken with the BOKU instrument.

3. Results and discussion

3.1. *Temperature correction of NO_2 DSCDs*

One of the aims of this study is to evaluate the seasonal cycle of NO_2 DSCDs obtained at the lowest elevation angles of MAX-DOAS measurements in Vienna. Due to the large temperature changes that occur during a full year, special care is necessary when thinking of the temperature dependence of the NO_2 absorption cross-section (see Sect. 2.1.5).

The temperature correction (Eq. (1)), which is introduced in Sect. 2.1.5, is applied to all DSCD NO_2 measurements retrieved in the visible spectral range and presented in this study. For demonstrating the difference between uncorrected and temperature-corrected NO_2 DSCDs obtained from the VETMED (Vis) measurements, we have selected the

Table 3
Air quality monitoring stations selected for use in the comparison with NO_2 DSCDs obtained from the lowest viewing directions of the two MAX-DOAS instruments. The stations are shown in Fig. 1.

	Lower Austria			Vienna				
	Klosterneuburg (B14)	Klosterneuburg (Wisentgasse)	Schwechat (Sportplatz)	A23 (Wehlistraβe)	AKH	Floridsdorf (Gerichtsgasse)	Gaudenzdorf	Hietzinger Kai
Latitudes	48° 18′ 29.6″	48° 18′ 8.0″	48° 08′ 42.0″	48° 12′ 11.0″	48° 13′ 10.3″	48° 15′ 39.9″	48° 11′ 13.7″	48° 11′ 18.1″
Longitudes	16° 19′ 40.6″	16° 19′ 15.0″	16° 28′ 28.0″	16° 26′ 4.4″	16° 20′ 44.0″	16° 23′ 49.0″	16° 20′ 21.6″	16° 18′ 0.1″

	Vienna						
	Hohe Warte	Kaiser-Ebersdorf	Kendlerstraβe	Schafberg	Stadlau	Stephansplatz	Taborstraβe
Latitudes	48° 14′ 56.4″	48° 09′ 24.1″	48° 12′ 18.0″	48° 14′ 7.3″	48° 13′ 34.9″	48° 12′ 29.3″	48° 13′ 0.3″
Longitudes	16° 21′ 25.5″	16° 28′ 33.8″	16° 18′ 35.1″	16° 18′ 5.6″	16° 27′ 30.0″	16° 22′ 23.7″	16° 22′ 51.3″

26 February 2018, which was the day within the period June 2017 to May 2018, when the lowest temperature (-13 °C) was measured at the BOKU weather station. In Fig. 4, uncorrected (gray curve) and temperature-corrected (blue curve) NO_2 DSCDs are shown for exemplary observations of the VETMED (AA = 254°, EA = 3°, solid lines) instrument, e.g. for the viewing direction pointing towards the location of the other instrument. This day with the lowest measured temperature was a weekday, with wind speeds ranging between 7 and 18 km h^{-1}. In the morning hours, when wind speeds were lowest, substantial NO_2 columns of about 1.15 x 10^{17} molecules cm^{-2} are derived after applying the temperature correction (blue curve). If not accounting for this correction, NO_2 DSCDs are overestimated by up to 15% in this case. This would have implications for the evaluation of seasonal cycles when considering potential occurrences of prolonged periods of cold weather like the one observed in January 2017 (monthly mean: -3.6 °C). Monthly means of air temperature for the winter months December, January, and February falling in the period that is evaluated in this study, are +2.9, +3.9, and -1.2 °C, respectively, resulting in lower values of monthly-averaged NO_2 DSCDs (about 7–8%) after applying the temperature correction. Interestingly, the highest percentage difference after temperature correction is observed for March (11.7%), where the monthly mean of measured air temperature was +3.5 °C. In contrast to the notable differences in winter, the effect of summer temperatures is negligibly small because of the temperature T_{ref} chosen.

3.2. Systematic comparison between MAX-DOAS path-averaged near-surface and in situ surface NO_2 VMRs

The relatively large number of air quality monitoring stations in the metropolitan area of Vienna, which deliver information on surface NO_2 concentrations (as well as VMRs after conversion, see Sect. 2.2.1), are the prerequisite for a systematic comparison with horizontal path-averaged NO_2 VMRs obtained from the two MAX-DOAS instruments.

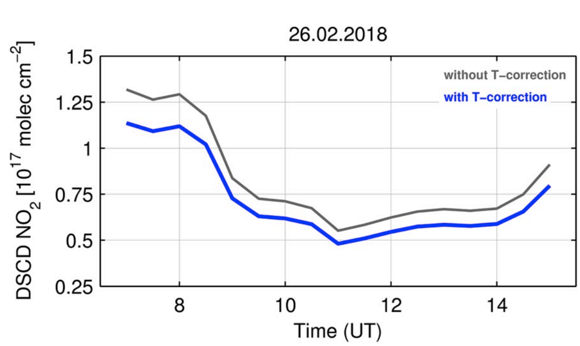

Fig. 4. NO_2 DSCDs obtained from the VETMED (AA = 254°, EA = 3°, solid lines) horizontal measurements in the visible spectral range on 26 February 2018. The gray and blue lines represent NO_2 DSCDs without and with temperature correction, respectively. (For interpretation of the references to color in this figure legend, the reader is referred to the Web version of this article.)

In Fig. 1, the geographical position of the selected air quality monitoring stations as well as the location of the two MAX-DOAS instruments are shown.

In a first step, the period 29 to 31 August 2017, e.g. three days with overall cloudless conditions, was chosen for a case study-based comparison between the two independent data sets. The wind was mainly blowing from southeastern directions throughout this period, in particular during daytime, with wind speeds reaching up to 20 km h^{-1} (not shown). As expected for such days with cloudless conditions, the measured global radiation at the surface level was highest during noon and overall characterized by a Gaussian shape. Time series of the mixing-height demonstrate a sharp increase during the morning hours with the maximum being reached around 15 UT in the afternoon (Fig. 5, middle panel). We note that for 30 August 2017, mixing-height data is not available after around 17 UT.

Time series of path-averaged near-surface NO_2 VMRs as obtained

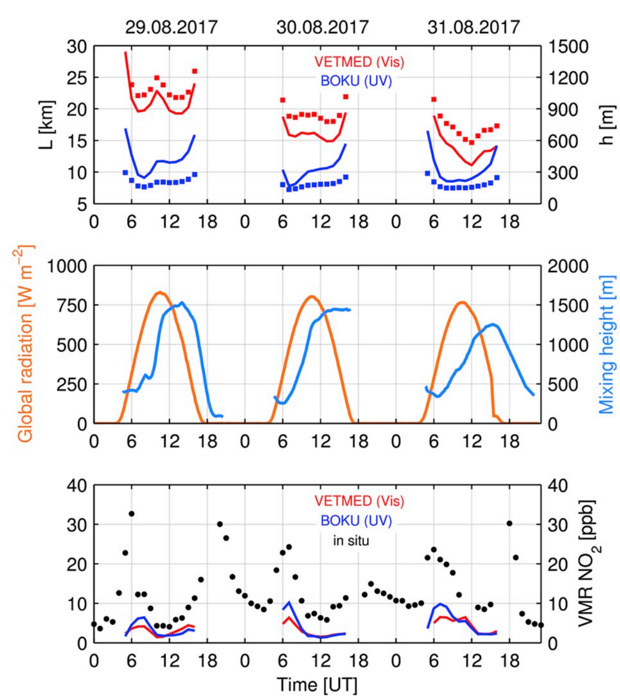

Fig. 5. Time series of L (solid line) and h (squares) of horizontal optical paths (upper panel), global radiation and mixing-height (middle panel), and path-averaged NO_2 VMRs from the VETMED (AA = 254°, EA = 3°, red line) and BOKU (AA = 74°, EA = 1°, blue line) MAX-DOAS instruments as well as surface NO_2 VMRs (black dots) from selected air quality monitoring stations (lower panel) for the period 29 August to 31 August 2017. The selection of air quality monitoring stations is given in Table 4. (For interpretation of the references to color in this figure legend, the reader is referred to the Web version of this article.)

from the VETMED (AA = 254°, EA = 3°) and BOKU (AA = 74°, EA = 1°) viewing directions that point towards the location of the other instrument indicate that highest amounts are observed in the morning hours, in particular on 30 and 31 August 2017 (Fig. 5, lower panel). The reasons for these elevated NO_2 amounts during that time of the day are shallow mixing-heights, low wind speeds, and possibly rush-hour traffic. The former two, which are both meteorological factors, influence the vertical and horizontal dilution of air pollutants, respectively (Aron, 1983). Lowest NO_2 VMRs are observed in the afternoon, most probably because of a pronounced horizontal and vertical dilution due to higher wind speeds and a fully developed mixing-height. The diurnal cycles of path-averaged NO_2 VMRs on those two days reflect the diurnal cycle of average surface NO_2 VMRs obtained from two air quality monitoring stations that are located between the two MAX-DOAS sites and in close proximity (<1.5 km) to the ground projected MAX-DOAS light path (Fig. 1). From Fig. 5, one can also see that there is a clear offset between NO_2 VMRs obtained from surface in situ measurements and from path-averaged near-surface MAX-DOAS observations. This is mostly due to the horizontal and vertical extension of light paths (Fig. 5, upper panel), resulting in observations of air masses reaching higher altitudes and areas outside the urban areas of Vienna, in addition to the air masses close to the surface and between the two measurement sites. It is interesting to note that the difference between the measurements of the two MAX-DOAS instruments is rather small, although not exactly the same air masses are observed. Differences in air masses observed result from several reasons: First, the effective light path of the VETMED instrument covers the lowest layer of the boundary layer due to the instruments location close to the ground level. In contrast, the MAX-DOAS instrument at the BOKU site is operating on a hill and thus, measuring almost 100 m above the ground level of the city center. Second, L is longer for the measurements taken with the VETMED instrument because of the fitting window in the visible spectral range. Third, also the geographical location of the two instruments is different and the sites are about 7.75 km apart from each other.

In order to further investigate the relationship between path-averaged near-surface NO_2 VMRs derived from the lowest viewing directions of the two MAX-DOAS instruments and surface NO_2 VMRs from air quality monitoring stations, a linear correlation analysis is applied. The relatively large number of air quality monitoring stations in and around Vienna makes it possible to perform this kind of analysis in a systematic way. For the following analysis, we only consider observations taken at SZA <75° in a first step and at the same time only those measurements, where the number of air quality monitoring stations within or close (<1.5 km) to the MAX-DOAS light paths is at least two. Moreover, the MAX-DOAS measurements are interpolated to the half-hour intervals of in situ measurements. For reasons of simplicity, constant effective light path lengths, following the recommendations made in Seyler et al. (2017), of 12.9 and 9.3 km are assumed for the Vis (VETMED) and UV (BOKU) instruments, respectively, to select air quality monitoring stations that are located within and/or close to the respective lowest viewing directions (see Fig. 1 and Table 4).

According to the above mentioned criteria, path-averaged NO_2 VMRs from a total of four (VETMED instrument) and three (BOKU instrument) lowest viewing directions are compared with averaged surface NO_2 VMRs measured by up to five air quality monitoring stations located within and/or close to the ground projected MAX-DOAS light paths. In order to remove MAX-DOAS measurements taken during unfavorable weather conditions (e.g. morning fog, broken clouds etc.), leading to unexpected high and/or low (sometimes even negative) O_4 DSCDs (see Seyler et al., 2017), the following filter criterion is defined for this analysis: Measurements taken under conditions with L > 75th percentile and L < 25th percentile are removed from the path-averaged NO_2 VMR data sets. This is a rough filter leading to a substantial removal of data (50%), considering the data set already filtered for SZA > 75°. It is important to note here that removing data above and below 75th and 25th percentile is not expected to affect the mean values in a systematic way.

The statistics (slope, intercept, and correlation coefficient) obtained from the linear correlation analysis are summarized in Table 4 for the selected viewing directions as well as for the four seasons. In summary, good agreement between the two independent data sets is found after applying the above mentioned filter criterion, in particular for the summer season, with correlation coefficients (R) ranging between 0.76 and 0.94. Interestingly, the highest correlation (R = 0.94) is identified between path-averaged NO_2 VMRs obtained from the VETMED instrument (AA = 254°, EA = 3°) and averaged surface NO_2 VMRs obtained

Table 4
Statistics calculated from the correlation between surface NO_2 VMRs obtained from selected air quality monitoring sites and VETMED (EA = 3°) and BOKU (EA = 1°) path-averaged NO_2 VMRs obtained from selected MAX-DOAS azimuthal angles. The slope, intercept, and correlation coefficient are calculated for the summer (JJA), fall (SON), winter (DJF), and spring (MAM) seasons of 2017/18. For better comparability, path averages taken at > 75th percentile and <25th percentile of L are removed from the data set, in addition to the removal of measurements taken at SZA >75° (see Sect. 3.2).

	VETMED MAX-DOAS vs. in situ NO_2				BOKU MAX-DOAS vs. in situ NO_2		
	AA = 170° [a]	AA = 225° [b]	AA = 254° [c]	AA = 300° [d]	AA = 74° [e]	AA = 137° [f]	AA = 213° [g]
slope							
summer (JJA)	0.178	0.171	0.279	0.255	0.310	0.239	0.198
fall (SON)	0.223	0.187	0.285	0.266	0.319	0.275	0.247
winter (DJF)	0.236	0.223	0.344	0.306	0.372	0.354	0.316
spring (MAM)	0.149	0.176	0.281	0.215	0.310	0.300	0.247
intercept							
summer (JJA)	0.212	-0.573	-0.102	-0.125	-0.163	-0.279	-0.868
fall (SON)	0.199	0.085	0.328	0.269	-0.122	0.049	-0.698
winter (DJF)	1.075	0.660	0.793	0.561	-0.103	-0.055	-0.427
spring (MAM)	0.830	-0.266	0.164	0.092	-0.056	-0.517	-0.982
correlation coefficient							
summer (JJA)	0.76	0.86	0.94	0.93	0.87	0.83	0.80
fall (SON)	0.73	0.75	0.86	0.85	0.88	0.80	0.84
winter (DJF)	0.60	0.69	0.81	0.82	0.87	0.85	0.82
spring (MAM)	0.69	0.77	0.89	0.85	0.84	0.85	0.82

[a] Selected air quality monitoring stations: Kaiser-Ebersdorf, Schwechat, Stadlau, A23/Wehlistraβe.
[b] Selected air quality monitoring stations: AKH, Gaudenzdorf, Hietzinger Kai, Stephansplatz, Taborstraβe.
[c] Selected air quality monitoring stations: Floridsdorf, Hohe Warte, Schafberg.
[d] Selected air quality monitoring stations: Floridsdorf, Klosterneuburg/Wiener Straβe, Klosterneuburg/Wiesentgasse
[e] Selected air quality monitoring stations: Floridsdorf, Hohe Warte.
[f] Selected air quality monitoring stations: AKH, Stephansplatz, Taborstraβe.
[g] Selected air quality monitoring stations: Hietzinger Kai, Kendlerstraβe, Schafberg.

from three stations that are located within and/or close to the respective horizontal light path. The correlation coefficient achieved for the BOKU instrument from the comparison of path-averaged NO_2 VMRs obtained from AA = 74° and EA = 1° with the average surface NO_2 VMRs from two air quality monitoring station is slightly lower (R = 0.87). In both cases, the viewing directions of the two MAX-DOAS instruments are the ones that point towards the location of the other instrument.

Scatter plots of these two cases showing high correlations in the summer season, but also the comparisons made for the other three seasons, are shown in Fig. 6. Also shown in that figure are scatter plots of path-averaged NO_2 VMRs and surface NO_2 VMRs, which are only filtered with respect to SZA >75° (gray dots). For example, there are many cases indicating comparatively low NO_2 amounts obtained with the MAX-DOAS instruments, whereas at the same time surface NO_2 VMRs show moderate to high values (and vice versa). This is related to measurements taken during unfavorable conditions in terms of atmospheric visibility (e.g. fog and broken clouds) and thus, the effective light path length of horizontal MAX-DOAS viewing directions is reduced (or enhanced), depending on which of the viewing directions is affected (zenith direction vs. low elevation).

The slopes of the linear correlation analysis after applying the above mentioned filter criterion, in addition to the SZA-filter (red and blue dots for the VETMED and BOKU instrument, respectively), are generally slightly lower for the comparisons made with measurements from the VETMED instrument (Fig. 6 and Table 4). The reason for this was already discussed above and can in general be attributed to differences in altitude, topography, geographical location as well as the horizontal and vertical extension of effective light paths. Overall, the slope values indicate that average NO_2 VMRs derived for the effective light path are about a factor of three smaller than those obtained from surface in situ NO_2 VMRs.

When comparing the slopes obtained from the selected horizontal light paths (see Table 4), it becomes clear that the viewing directions of both MAX-DOAS instruments pointing towards the city center (AA = 225°, EA = 3° and AA = 137°, EA = 1°) are associated with lower values than the viewing directions pointing towards the location of the other instrument. Following the same logics as above, the horizontal variability appears to be much larger at the surface level than at the elevated layers covered by the MAX-DOAS light paths, arguably because of air mass mixing. In fact, NO_2 is diluted as soon as wind speeds increase and mixing-heights start to develop after sunrise. Path-averaged NO_2 VMRs obtained from the VETMED instrument's viewing direction pointing towards the city center (AA = 225°, EA = 3°) are compared with averages of surface NO_2 VMRs obtained from five stations, all of them located close to the city center and rather distant (>5 km) from the VETMED instrument.

A similar comparison between ground-based CMAX-DOAS tropospheric NO_2 vertical column densities and surface NO_2 VMRs is presented in Kramer et al. (2008). In addition to the fact that the authors of that study used tropospheric NO_2 VCDs instead of path-averaged NO_2 VMRs from horizontal viewing directions, the linear correlation analysis in their study is based on daily averages computed for the winter season. The results of Kramer et al. (2008) indicate a positive offset between CMAX-DOAS and in situ measurements for those stations operating in urban areas and in sectors with heavy traffic density, whereas a negative intercept is found for those stations associated with urban background conditions.

Interestingly, negative offsets in our study are found for all azimuthal viewing directions of the BOKU instrument, with highest negative intercept values derived for AA = 213°. We note that this azimuthal viewing direction is pointing towards the location of the air quality monitoring station (Hietzinger Kai) repeatedly showing the highest values in Vienna. Moreover, this in situ station is the only one in Vienna that exceeded the European limit values for annual average NO_2 concentrations (Augustyn et al., 2018). While this air quality monitoring station is operating next to a high traffic road that passes perpendicularly to the MAX-DOAS light path, the rest of the light path covers rather residential areas. Therefore, the relatively high negative offset obtained for this viewing direction clearly makes sense in this case, following the reasoning in Kramer et al. (2008).

3.3. Seasonal cycles of L and path-averaged NO_2, HCHO, and CHOCHO VMRs

For the evaluation of seasonal cycles of L, as well as path-averaged NO_2, HCHO, and CHOCHO VMRs, data from both MAX-DOAS

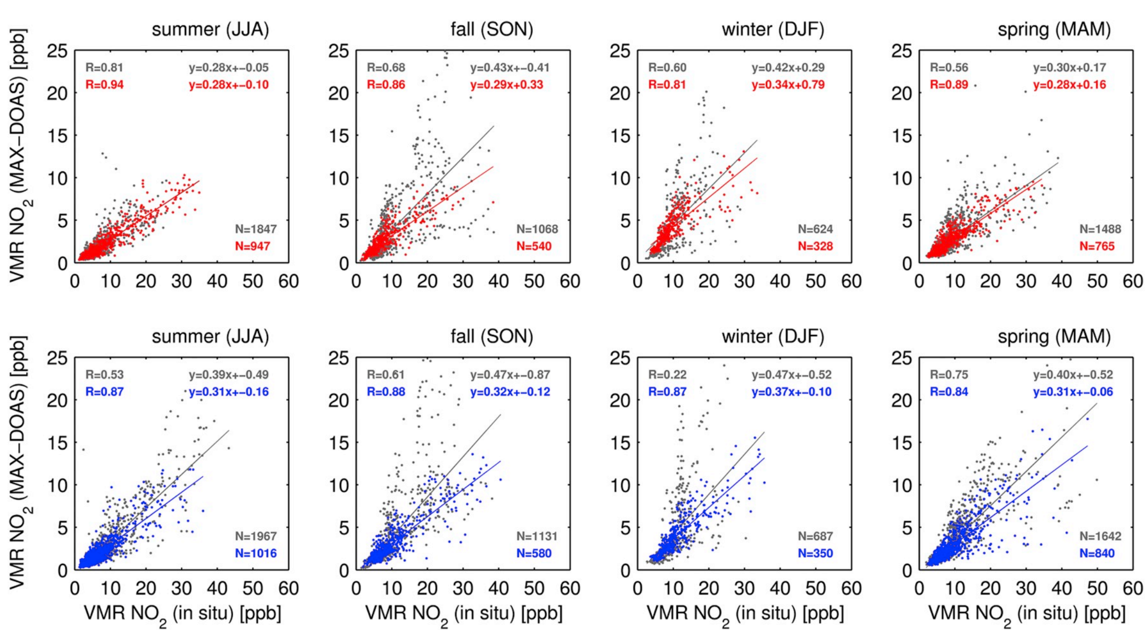

Fig. 6. Path-averaged NO_2 VMRs retrieved from the VETMED (AA = 254°, EA = 3°, upper panels) and BOKU (AA = 74°, EA = 1°, lower panels) MAX-DOAS observations plotted against NO_2 surface VMRs from selected air quality monitoring stations (see Fig. 1 and Table 4). Measurements taken at SZA <75° and interpolated to half-hour intervals are shown in red (VETMED) and blue (BOKU). Gray dots represent measurements removed by the filter criterion (see Sect. 3.2). (For interpretation of the references to color in this figure legend, the reader is referred to the Web version of this article.)

instruments spanning the period June 2017 to May 2018 are used. Monthly means are computed by averaging all daytime measurements, without any data filtering. As already outlined in Sect. 2.1.3, the analysis is based on spectral measurements taken at the lowest possible elevation angles from the VETMED (EA = 3°) and BOKU (EA = 1°) instruments.

Seasonal cycles of L obtained from the MAX-DOAS viewing directions pointing towards the location of the other instrument are shown in Fig. 7 (upper panels). As expected, highest monthly-averaged L are observed before and after mid-summer, at a time when daytime mixing-heights are high and situations with foggy situations are generally absent. Nevertheless, other factors such as aerosol vertical profiles affect the atmospheric visibility and thus, the length of the effective light path (Sinreich et al., 2013; Wang et al., 2014). During the winter months, however, it appears that L is unusually large in December and small in January and February. The reason for this might be untypically good and poor visibility conditions, respectively, which is confirmed by the meteorological data recorded by the BOKU weather station (not shown). On the one hand, many days with undisturbed global radiation measurements are found in December, suggesting that visibility conditions have been good. On the other hand, reduced global radiation is found for many days in January and February, probably caused by fog and/or thick, low clouds.

In Fig. 7 (middle panels), the results are presented for path-averaged NO_2 VMRs. Overall, highest monthly means of NO_2 amounts are observed in November, January, February, and March, when considering both the temperature-corrected (VETMED instrument only) and non-corrected curves of the two instruments. This is in good agreement with seasonal NO_2 cycles obtained from MAX-DOAS measurements as presented in Ma et al. (2013) and in Hendrick et al. (2014) for Beijing (China), in Gratsea et al. (2016) for Athens (Greece), in Wang et al. (2017) for Wuxi (China) and in Chan et al. (2018) for Hong Kong, where highest monthly averages of NO_2 column amounts are also found during the winter season. In January and February, but in particular in December, computed averages in our study are smaller than someone would expect from the overall shape of the seasonal cycle. Possible reasons for this could be meteorological factors affecting the dilution of NO_2. In fact, January and February 2018 were characterized by relatively warm temperatures and a substantial number of days with precipitation. Moreover, the number of days with cloudless skies and good visibility was rather low for those two months. In contrast, unusually good visibility conditions were observed in December, leading to relatively high L values and at the same time relatively low path-averaged NO_2 VMRs.

When comparing the monthly means of path-averaged NO_2 VMRs obtained from the VETMED instrument (left) with the ones from the BOKU instrument (right), it is apparent that the values of the former are slightly lower than the latter ones. There are many possible reasons for this difference, which have already been discussed above: first of all, the VETMED instrument is located about 7.75 km to the east of the BOKU instrument in a different surrounding area. Second, the former instrument is situated about 100 m lower than the latter one. Third, and probably most importantly, the VETMED and BOKU instruments are measuring in the Vis and UV spectrum, respectively, with longer effective light paths and thus, larger slant column amounts obtained for the

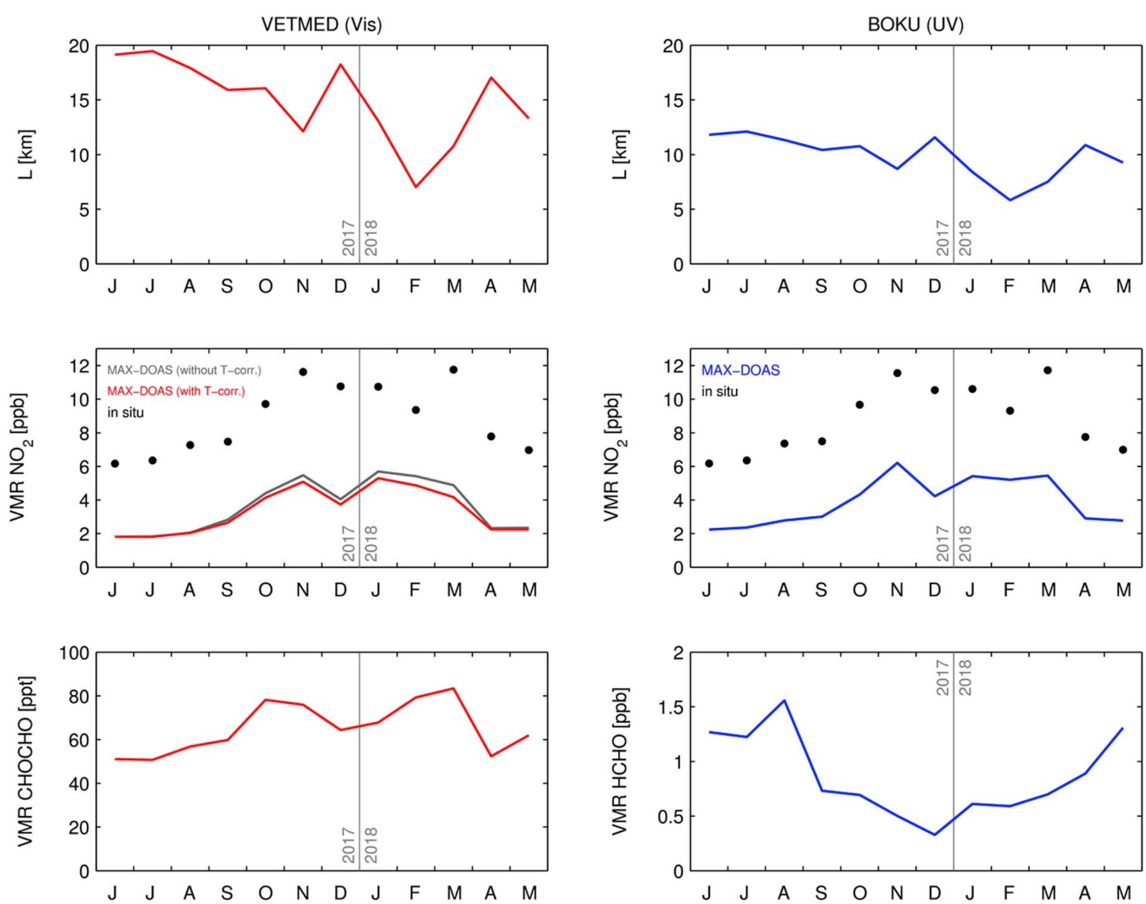

Fig. 7. Seasonal cycles of effective light path length (L) (upper) as well as path-averaged NO_2 (middle), HCHO, and CHOCHO (lower) VMRs from June 2017 to May 2018. Monthly-averaged values at AA = 254° and EA = 3° (VETMED instrument, left panels) and at AA = 74° and EA = 1° (BOKU instrument, right panels) are represented by red and blue curves, respectively. The monthly means are calculated by taking the average of unfiltered daytime measurements. The gray curve and black dots in the middle panels show path-averaged NO_2 VMRs without temperature corrections and averaged surface VMRs from in situ stations, respectively (see Table 4). (For interpretation of the references to color in this figure legend, the reader is referred to the Web version of this article.)

VETMED instrument, in particular when considering horizontal observations as evaluated in this study. The comparison between path-averaged NO_2 VMRs and surface in situ NO_2 VMRs (see Fig. 7 middle panels) shows that the former are about a factor of three smaller than the latter ones, which is in overall good agreement with the findings of Sect. 3.2.

The seasonal cycle of path-averaged HCHO VMRs is characterized by high values during summer season and low values during the winter season (Fig. 7, lower right). This is in good agreement with seasonal HCHO cycles obtained from MAX-DOAS observations as presented in Gratsea et al. (2016) for Athens (Greece) and in Wang et al. (2017) for Wuxi (China). In both studies, highest monthly averages of HCHO

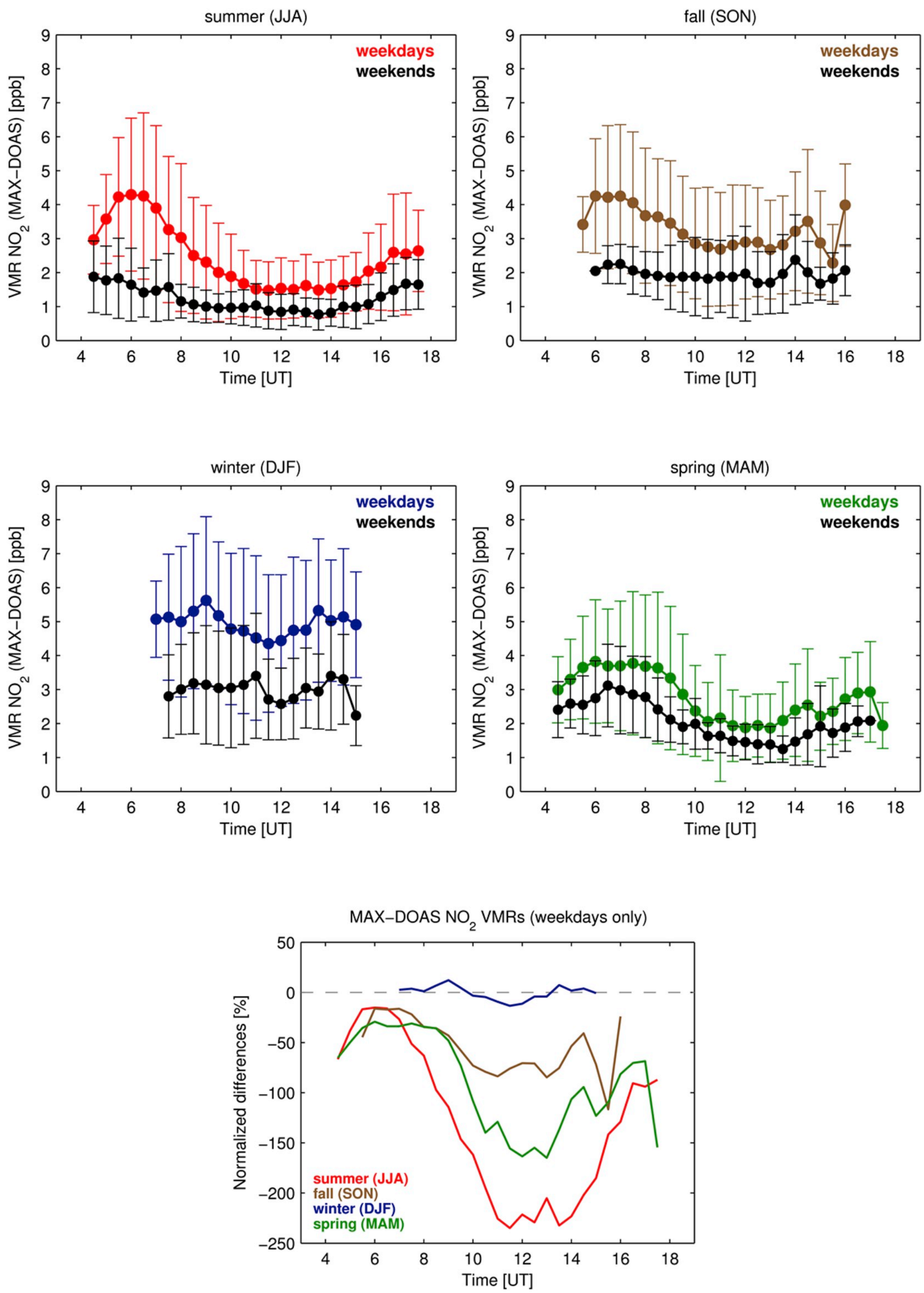

Fig. 8. Averaged diurnal cycles of path-averaged NO_2 VMRs for the summer (JJA), fall (SON), winter (DJF), and spring (MAM) season. The colored and black dots represent half-hour averages of VMRs obtained from the VETMED instrument (EA = 3°, AA = 225°) on weekdays and weekends, respectively. The first and last 30-min intervals are discarded because of too low numbers of measurements. Moreover, path averages taken at > 75th percentile and <25th percentile of L are removed from the data set (see Sect. 3.2). Error bars represent the standard deviation. Normalized differences of path-averaged NO_2 VMRs are calculated for weekdays only and with respect to the seasonally-averaged daily mean of the winter (DJF) season.

column amounts are also observed during the summer season. In our study, monthly means of path-averaged HCHO VMRs are larger in summer than in winter by a factor of up to four. In comparison, much less seasonal variability is found over Athens and Wuxi. This might be explained by the geographical location of the two urban agglomerations, which is in the Subtropics, having warmer temperatures in winter and thus, more HCHO production during that time of the year.

A different seasonal cycle than for NO_2 and HCHO is observed for CHOCHO mixing ratios (Fig. 7, lower left). Highest monthly averages show up during fall and late winter/early spring. In contrast to the NO_2 cycle, peak values of CHOCHO occur slightly earlier and later in fall and winter, respectively. This finding suggests that significant amounts of CHOCHO are related to anthropogenic emission sources in the urban environment of Vienna, in addition to the formation from precursor VOC species. To the authors' best knowledge, a seasonal CHOCHO cycle obtained from MAX-DOAS measurements is so far only documented for Athens (Gratsea et al., 2016). The authors of that study also report that CHOCHO amounts are more strongly linked to anthropogenic sources than HCHO, which is supported by the findings of our study.

3.4. Diurnal cycles of path-averaged NO_2, HCHO, and CHOCHO VMRs

Diurnal cycles of path-averaged NO_2, HCHO, and CHOCHO VMRs are computed for the summer, fall, winter, and spring seasons (2017/18) by averaging all daytime measurements and applying the above mentioned filter criterion (see Sect. 3.2). In order to evaluate the difference between weekdays and weekends, the averaging procedure is separately performed for Mondays till Fridays (weekdays) as well as for Saturdays and Sundays (weekends). Public holidays are not specifically considered for this analysis.

In Fig. 8, seasonally averaged NO_2 diurnal cycles are shown for measurements taken with the VETMED instrument (AA = 225°, EA = 3°). For fall and spring, but in particular for the summer season, distinct morning peaks can be clearly identified. The explanations for such high morning values in Vienna, which were already mentioned in Sect. 3.1, are associated with low wind speeds, a shallow mixing-height, and morning rush-hour traffic. Path-averaged NO_2 VMRs obtained on weekdays can be higher than on weekends by a factor of up to 2.5 on average, in particular during morning hours of the summer and fall seasons. Because of the shortened sunshine duration in winter, morning and evening NO_2 peaks are less pronounced as rush hours are not covered by the measurements. The less pronounced NO_2 winter peaks could also be attributed to emissions from domestic heating, which are released rather continuously throughout the whole day. The daily distribution of traffic density on Viennese roads as investigated for the year 2015 can be found at https://www.wien.gv.at/stadtentwicklung/studien/pdf/b008495.pdf. Compared to the other seasons, noon time averages of path-averaged NO_2 VMRs obtained on working days are higher and well above 4 ppb during winter months. As already mentioned in Sect. 3.3, the averaged NO_2 amounts presented in Fig. 7 might be lower than expected for this coldest season of the year due to the unusually warm temperatures and low visibility in January and February 2018. Calculated percentage differences between seasonally averaged daytime averages of NO_2 VMRs on weekdays and corresponding daytime averages on weekends are -50% (summer), -41% (fall), -40% (winter), and -26% (spring). Averaged diurnal cycles of path-averaged NO_2 VMRs obtained from the BOKU instrument (AA = 137°, EA = 1°) are very similar in shape, but slightly higher in magnitude (not shown). Similar diurnal NO_2 cycles in terms of the shape were obtained from horizontal MAX-DOAS viewing directions (EA = 1°) in Athens (Gratsea et al., 2016). In a further step, normalized differences of path-averaged NO_2 VMRs are computed for weekdays only and with respect to the seasonally-averaged daily mean of the winter season (Fig. 8). While morning values of path-averaged NO_2 VMRs in summer, fall, and spring are up to 60% lower than the winter mean, substantially lower values are observed around noon, in particular during summer and spring (up to 250%). The main reason for this might be the larger mixing-height during that time of day and year, leading to increased horizontal and vertical mixing of pollutants.

Seasonally averaged diurnal cycles of path-averaged HCHO VMRs are presented in Fig. 9 for the summer, fall, winter, and spring seasons (2017/18). Overall, the diurnal variation of HCHO is slightly less pronounced than for NO_2. Moreover, the differences between weekdays and weekends are smaller, but still apparent. Calculated percentage differences between seasonally averaged daytime averages of HCHO VMRs on weekdays and corresponding daytime averages on weekends are -19% (summer), -8% (fall), -9% (winter), and +22% (spring). Interestingly, the averaged HCHO mixing ratios are lower on weekdays than on weekends in spring. This is an indication that HCHO might not be primarily produced from anthropogenic sources and thus, mainly meteorological factors could affect the production of HCHO in Vienna. Incidentally, highest temperatures in March and April were recorded on weekend days (not shown). Normalized differences indicate that at any time of the day, path-averaged HCHO VMRs as obtained from the horizontal MAX-DOAS measurements for summer and spring are substantially larger than the calculated winter mean (see Fig. 9, lower panel).

Averaged diurnal cycles similar to those observed for NO_2 are identified for CHOCHO (Fig. 10). Highest averaged CHOCHO amounts are found during the morning hours. The ratio of the path-averaged CHOCHO VMRs between weekdays and weekends is less than a factor of two and thus, slightly less pronounced than for NO_2. This is generally in good agreement with the results presented in Gratsea et al. (2016). However, CHOCHO peak values in Athens show up a few hours later than in Vienna, around noon, and also later in time than maxima of NO_2 DSCDs are observed, which is not observed for Vienna, where both NO_2 and CHOCHO maxima are found almost at the same time. Calculated percentage differences between seasonally averaged daytime averages of CHOCHO VMRs on weekdays and corresponding daytime averages on weekends are -35% (summer), -28% (fall), -32% (winter), and -4% (spring). Interestingly, normalized differences of path-averaged CHOCHO VMRs are similar in shape with those of NO_2 VMRs, but much lower in magnitude.

3.5. Azimuthal dependence of path-averaged NO_2, HCHO, and CHOCHO VMRs

Horizontal differences of trace gas amounts over the urban area of Vienna are evaluated in two steps. First, seasonal means of path-averaged NO_2, HCHO, and CHOCHO VMRs with their corresponding standard deviation are calculated for the lowest elevation angles of the individual azimuthal viewing directions of the VETMED (EA = 3°) and BOKU (EA = 1°) instruments. As already mentioned in Sect 3.2, the filter criterion is applied for this analysis, meaning that measurements with L > 75th percentile and L < 25th percentile are removed from the path-averaged trace gas VMR data sets. Second, path-averaged NO_2 VMRs obtained from the individual lowest viewing directions of the VETMED instrument and interpolated to half-hour intervals are correlated against those path-averaged NO_2 VMRs derived from the individual lowest viewing directions of the BOKU instrument. Such a correlation analysis can only be made for NO_2 in our study as this trace gas is retrieved from both the VETMED (Vis) and BOKU (UV) spectrometers. The above mentioned filter criterion is also applied for this analysis.

The results of the former analysis are summarized in Fig. 11 and Fig. 12 for path-averaged NO_2 VMRs and L, respectively, obtained from the VETMED (left) and BOKU (right) instruments as well as in Fig. 13 for path-averaged CHOCHO VMRs from the VETMED (left) and HCHO VMRs from the BOKU (right) instruments.

Highest (lowest) seasonally-averaged daytime averages of NO_2 amounts are observed for winter (summer) with both the VETMED and BOKU instruments (see also Sect. 3.3). A longer lifetime of NO_2 as well as lower mixing-heights during that time of the season might be the main reason. Moreover, emissions from domestic heating could also explain

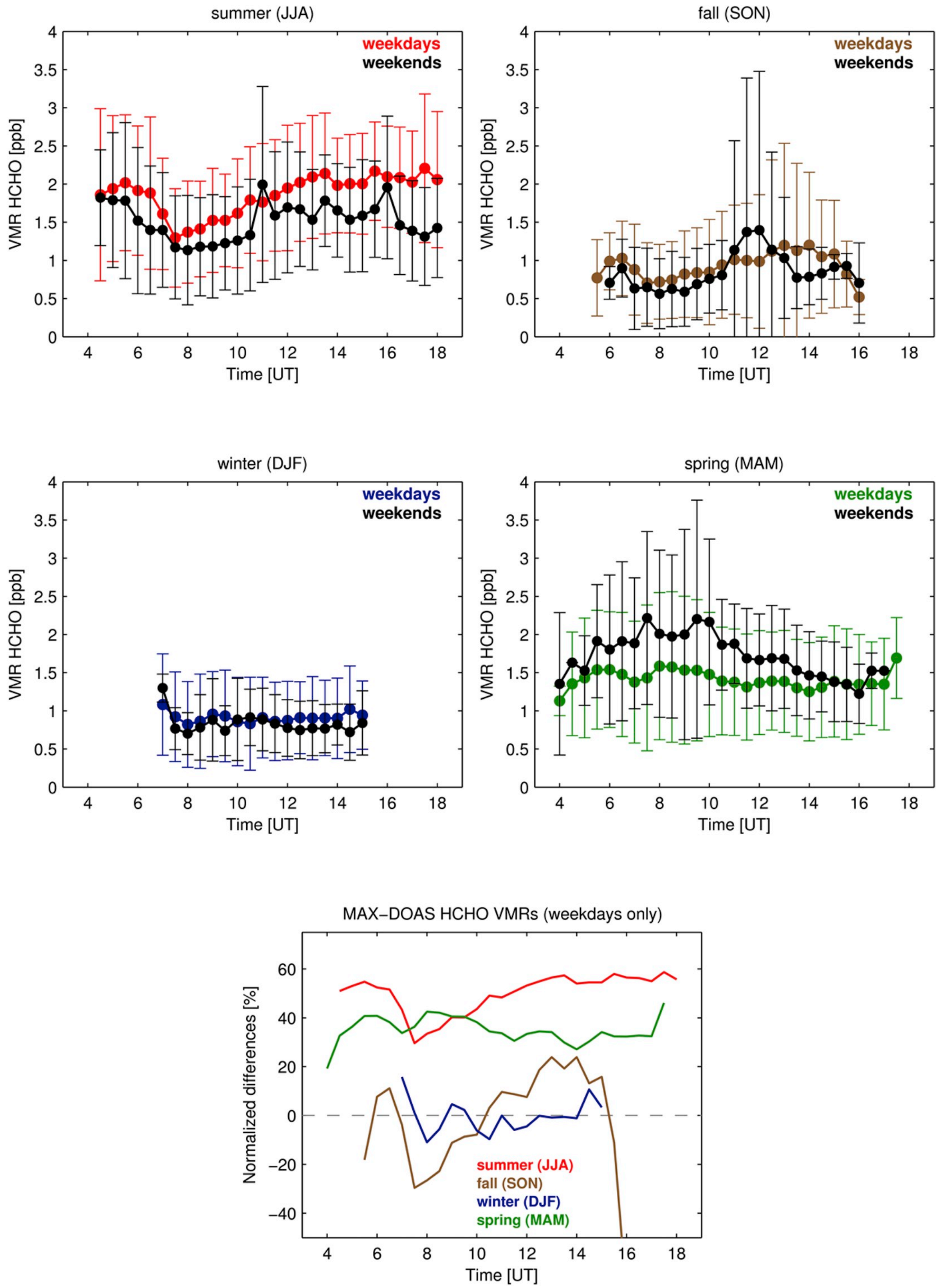

Fig. 9. Same as Fig. 8, but for path-averaged HCHO VMRs obtained from the BOKU instrument (EA = 1°, AA = 137°).

elevated NO_2 amounts in winter. When the averaged NO_2 amounts obtained from the different horizontal viewing directions are compared with each other, it becomes clear that the highest values are found when the instruments are pointing towards or close to the city center, which is valid for all seasons. The means of NO_2 VMRs for those azimuthal viewing directions are slightly lower than 5 ppb for the VETMED instrument and slightly higher than 5 ppb for the BOKU instrument during fall and winter. Moreover, the variability of seasonally averaged NO_2 VMRs is generally low when those horizontal viewing directions pointing towards the urban area are compared with each other. The variability of averaged NO_2 amounts between the different seasons appears generally larger for the BOKU than for the VETMED instrument, which might be caused by smaller seasonal fluctuations of O_4 DSCDs and thus, also smaller fluctuations of L in the UV range (see Fig. 12).

The overall pattern of seasonally-averaged path-averaged CHOCHO VMRs is quite similar to that observed for NO_2 with highest values obtained when the VETMED instrument is pointing towards the city center and/or towards the South (e.g. busy roads and industry). Again, this finding suggests that CHOCHO over the urban area of Vienna seems to be dominantly from anthropogenic origin or from the oxidation of

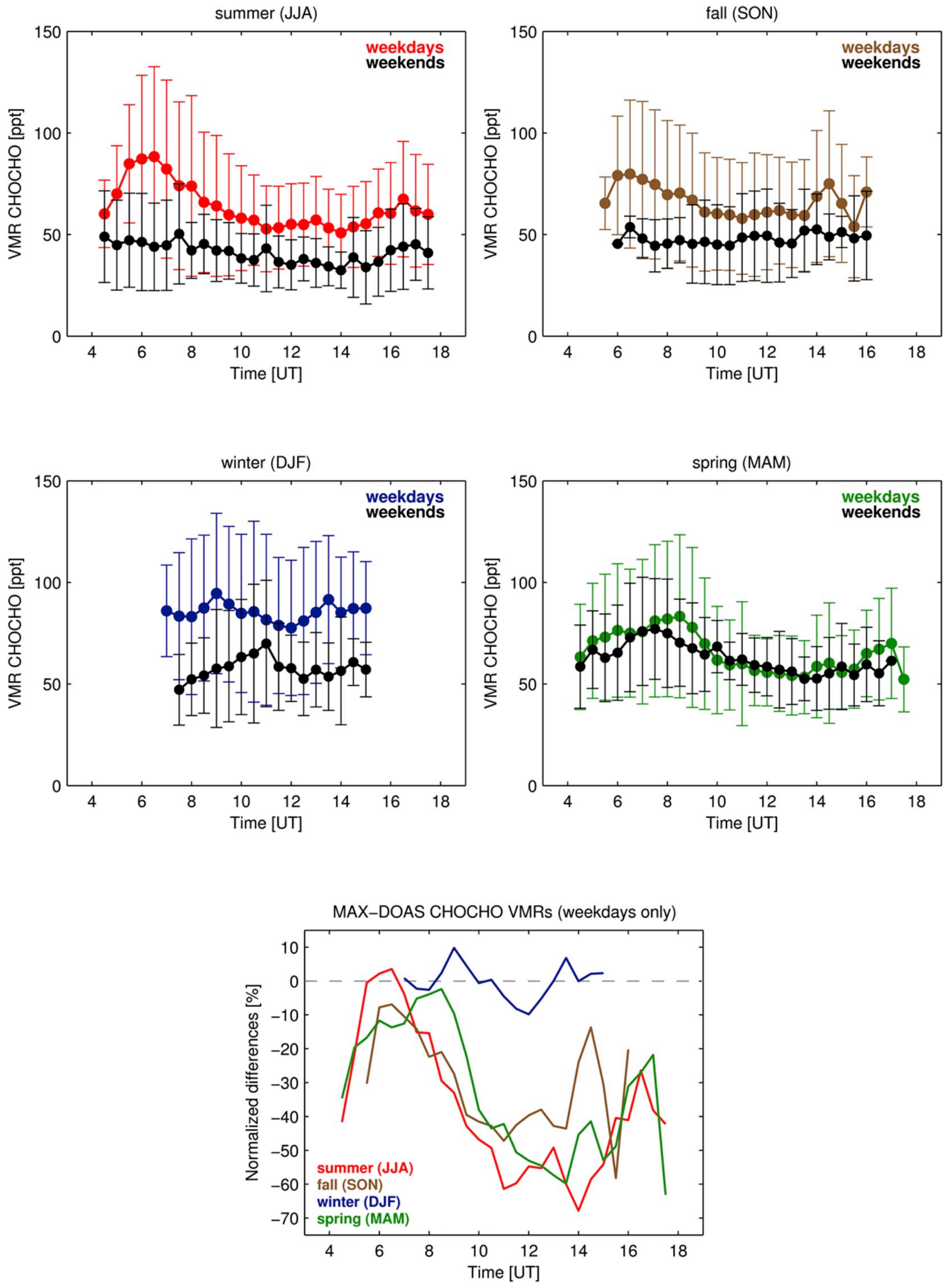

Fig. 10. Same as Fig. 8, but for path-averaged CHOCHO VMRs obtained from the VETMED instrument (EA = 3°, AA = 225°).

anthropogenic VOCs. As already mentioned for NO_2, path-averaged CHOCHO VMRs are highest during the winter season (see Fig. 13, left). We note that this is contrast with the results presented in Fig. 7, where highest CHOCHO are found rather in fall and early spring than in winter. The reason for this difference is that the results presented in Fig. 7 are based on unfiltered data.

In contrast to the azimuthal dependence observed for path-averaged NO_2 and CHOCHO VMRs, where the highest values are measured towards the city center, HCHO amounts obtained from the lowest viewing direction are higher towards the location of the VETMED site, in particular during the summer season. One reason for this could be increased biogenic HCHO production from vegetation on the Danube Island, which is partly covered by this viewing direction. Again, this finding implies that HCHO, unlike NO_2 and CHOCHO, is not primarily produced from anthropogenic sources in the city center of Vienna during that time of the year.

The correlation coefficients obtained from the linear correlation analysis are listed in Table 5. As expected, the highest correlation coefficient ($R = 0.91$) of NO_2 amounts obtained from horizontal viewing directions of the two instruments is found between AA = 254° (VETMED instrument) and AA = 74° (BOKU instrument) when the instruments point towards each other. A high correlation coefficient ($R = 0.89$) are

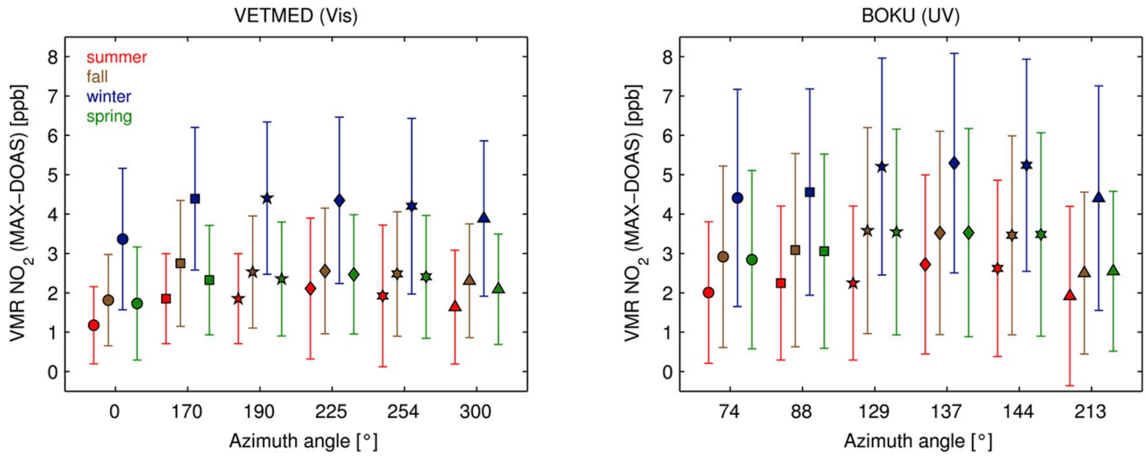

Fig. 11. Azimuthal dependence of seasonally-averaged path averages of NO_2 VMRs at EA = 3° (VETMED instrument, left) and at EA = 1° (BOKU instrument, right) for the summer (JJA), fall (SON), winter (DJF), and spring (MAM) seasons of 2017/18. The error bars represent the standard deviation. Moreover, path averages taken at > 75th percentile and <25th percentile of L are removed from the data set, in addition to the removal of measurements taken at SZA >75° (see Sect. 3.2).

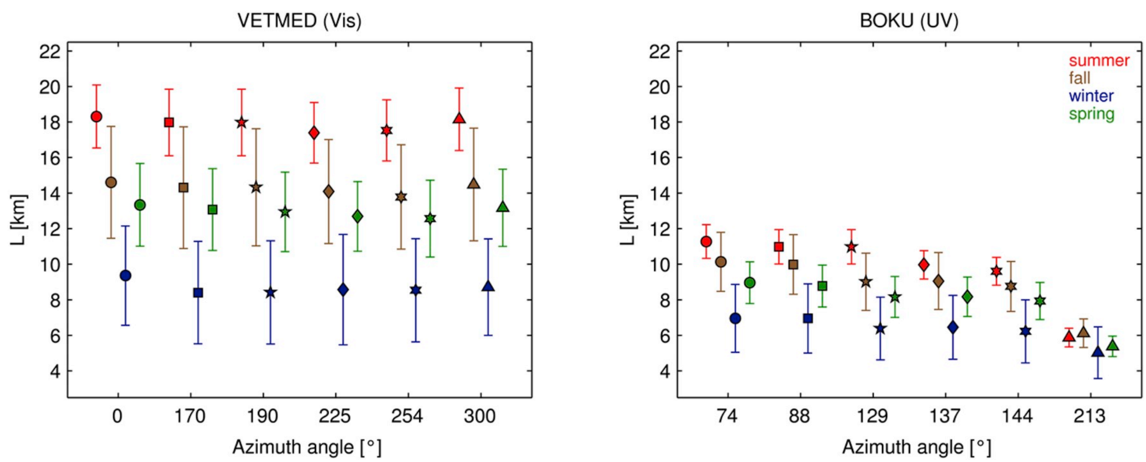

Fig. 12. Same as Fig. 11, but for seasonally-averaged effective light path lengths (L) at EA = 3° (VETMED instrument, left) and EA = 1° (BOKU, right).

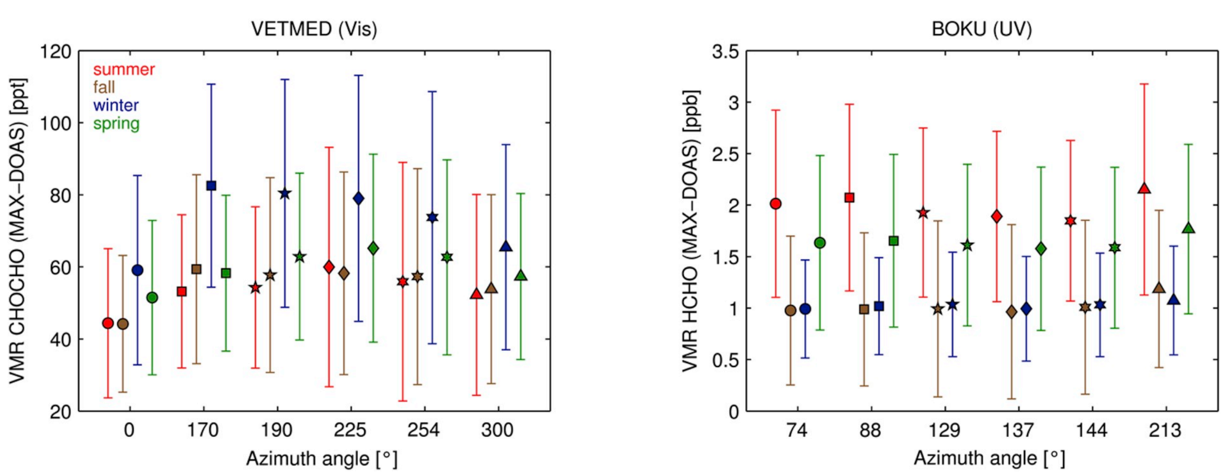

Fig. 13. Same as Fig. 11, but for seasonally-averaged path averages of CHOCHO VMRs at EA = 3° (VETMED instrument, left) and HCHO VMRs at EA = 1° (BOKU instrument, right).

also found when path-averaged NO_2 VMRs obtained from AA = 225° (VETMED instrument) are compared with those obtained from AA = 137° (BOKU instrument), e.g. both viewing directions pointing towards the city center. In contrast, the lowest correlation coefficient (R = 0.66) is observed when AA = 170° (VETMED instrument) is compared with AA = 213° (BOKU instrument). While AA = 170° (VETMED instrument) covers rather industrial sectors and high-traffic roads in the Southeast of the city center, AA = 213° (BOKU instrument) is pointing towards

Table 5
Correlation coefficients obtained from the linear correlation between path-averaged NO_2 VMRs obtained from individual azimuthal measurements (interpolated to 30-min intervals) of the VETMED (EA = 3°) and BOKU (EA = 1°), based on a full year (from June 2017 to May 2018). For better comparability, path averages taken at > 75th percentile and <25th percentile of L are removed from the data set, in addition to the removal of measurements taken at SZA >75° (see Sect. 3.2).

	VMR NO2	VETMED Vis (EA = 3°)					
		AA = 0°	AA = 170°	AA = 190°	AA = 225°	AA = 254°	AA = 300°
BOKU UV (EA = 1°)	AA = 74°	0.845	0.780	0.820	0.902	0.914	0.899
	AA = 88°	0.833	0.806	0.832	0.899	0.904	0.885
	AA = 129°	0.754	0.786	0.828	0.880	0.865	0.807
	AA = 137°	0.780	0.803	0.844	0.885	0.868	0.814
	AA = 144°	0.776	0.801	0.843	0.890	0.874	0.813
	AA = 213°	0.694	0.658	0.737	0.863	0.889	0.807

residential areas more generally. In addition, both viewing directions are pointing almost in parallel towards South, but at a distance of about 7.75 km from each other, covering completely different air masses.

3.6. *Wind dependence of path-averaged NO_2, HCHO, and CHOCHO VMRs*

As already found in a recent case study (Schreier et al., 2019), the horizontal NO_2 distribution over the urban area of Vienna is largely driven by local wind conditions during daytime. In order to evaluate the effect of wind direction and wind speed on NO_2, HCHO, and CHOCHO amounts in a statistical manner in this study, 10-min averages of the two wind parameters as well as higher temporally resolved path-averaged NO_2, HCHO, and CHOCHO VMRs as obtained from the viewing directions pointing towards the city center of Vienna (AA = 225°, EA = 3° for the VETMED and AA = 137°, EA = 1° for the BOKU instrument) are linearly interpolated to 30-min intervals. We investigated the amounts of NO_2, HCHO, and CHOCHO for two different wind conditions, which are characteristic for the summer season in Vienna: Winds from the west and winds from the Southeast.

The results obtained for path-averaged NO_2 VMRs from the VETMED (AA = 225°, EA = 3°) and BOKU (AA = 137°, EA = 1°) instruments are presented in the upper and lower panels of Fig. 14, respectively. The mean (red plus sign), median (red line), 25th (75th) percentile (blue box), and 9th (91st) percentile (gray whiskers) values indicate that there is a clear dependence of NO_2 amounts on wind direction. When the wind is blowing from the west, bringing rather clean air to the city center of Vienna, path-averaged NO_2 VMRs are generally low (upper and lower left panels). Path-averaged NO_2 VMRs obtained from both instruments are in very good agreement, but slightly higher for the BOKU instrument. Moreover, the wind speed plays only a minor role in this case. In contrast, a large dependence on wind speed is observed for cases with winds blowing from the Southeast. Highest path-averaged NO_2 VMRs with mean values reaching about 4.5 ppb (VETMED instrument) and 7 ppb (BOKU instrument) are found when low wind speeds occur (0–5 km h^{-1}). Path-averaged NO_2 VMRs are decreasing with increasing wind speeds. These findings are consistent with results presented in Schreier et al. (2019), where highest NO_2 amounts close to the city center were also recorded on days with winds from the Southeast. The explanation for this is that most of the industry and power plants are located in the southeast of the city center. Moreover, heavily frequented motorways are also situated in this area. While NO_2 amounts are also clearly affected by the wind direction in Athens (Gratsea et al., 2016), the dependence seems to be less strong in Wuxi (Wang et al., 2017), with the exception of the winter season.

The effect of wind direction and wind speed on path-averaged HCHO VMRs is presented in Fig. 15. As observed for NO_2, HCHO amounts are generally higher when the wind is blowing from the Southeast.

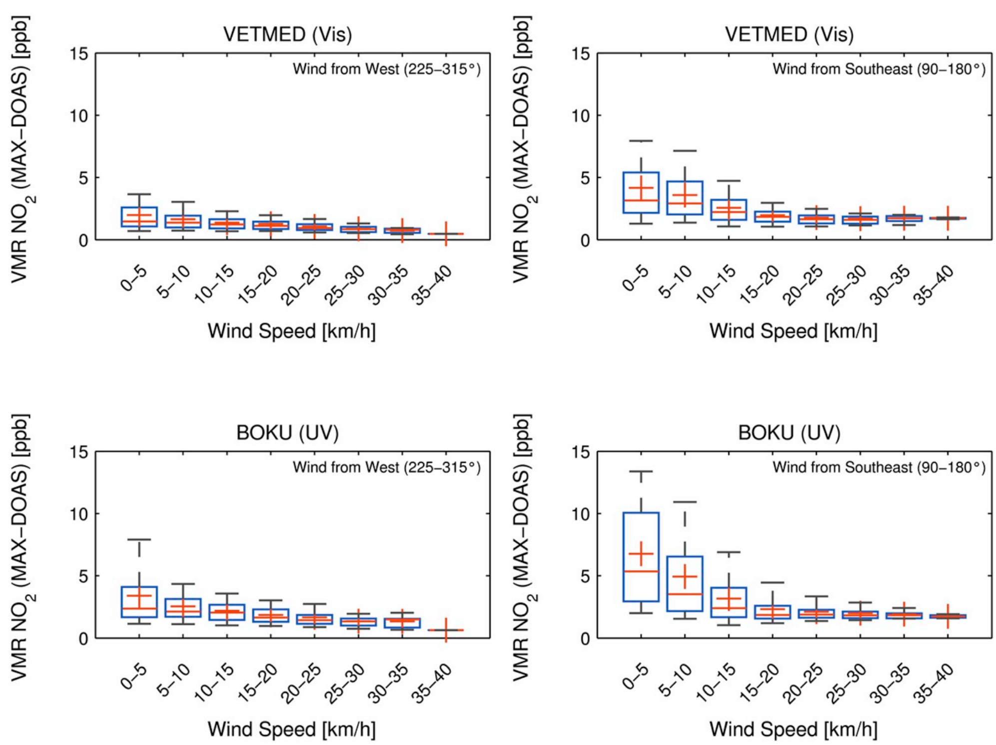

Fig. 14. Path-averaged NO_2 VMRs obtained from the VETMED (EA = 3°, AA = 225°, upper panels) and BOKU (EA = 1°, AA = 137°, lower panels) instruments as a function of wind speed during the summer (JJA) season. The left and right panels demonstrate cases with wind directions from the West and Southeast, respectively.

Interestingly, highest mean values of HCHO during such cases show up when the wind speeds are between 5 and 10 km h^{-1}, in addition to the interval with calm winds. While the effect of wind speed on VMRs for cases with winds blowing from the west was rather low for NO_2, a slightly more distinct dependence is observed for HCHO. This again highlights the fact that HCHO is not entirely produced from anthropogenic emission sources over the urban environment of Vienna. Air masses coming from the west of Vienna are rather related to the oxidation of biogenic NMVOCs. Nevertheless, higher VMRs on days with winds from the southeast indicate that HCHO over the urban environment of Vienna additionally results from the oxidation of anthropogenic NMVOCs. In summary, the effect of wind direction and wind speed is less strong than observed for NO_2, suggesting that local anthropogenic emission sources might be less relevant for HCHO in Vienna. This is in good agreement with the findings reported in Gratsea et al. (2016) and Wang et al. (2017), where the effect of wind conditions is also less strong for columnar HCHO amounts than for NO_2 amounts.

As already found for the diurnal cycles (Sect. 3.4), a strong similarity between NO_2 and CHOCHO is also observed for the relationship between wind conditions and trace gas amounts. While air masses from the west are related with lower CHOCHO amounts, increased path-averaged CHOCHO VMRs are observed when the wind is blowing from southeast (Fig. 16). According to these findings, it seems that CHOCHO is predominantly formed from VOCs emitted by anthropogenic sources, which is in good agreement with the conclusions drawn in Gratsea et al. (2016).

4. Summary and conclusions

In December 2016 and May 2017, two MAX-DOAS instruments were installed at two different locations in the northeast (VETMED site) and northwest (BOKU site) of Vienna. Since then the VETMED (Vis) and BOKU (UV) instruments continuously take daytime spectral measurements at selected viewing directions, each of the two instruments including one azimuthal viewing direction towards the city center and one towards the location of the other instrument.

A set of data encompassing one year of simultaneous measurements from the two instruments, covering the four seasons summer (JJA), fall (SON), winter (DJF), and spring (MAM) of the years 2017 and 2018, are reported in this study. Several analyses have been performed on this data set in order to gain insights into the horizontal distributions of path-averaged near-surface CHOCHO, HCHO, and in particular of NO_2 volume mixing ratios (VMRs) as retrieved from the lowest possible viewing directions of the two MAX-DOAS instruments.

The first analysis focuses on the systematic comparison between path-averaged NO_2 VMRs derived from the lowest viewing directions of the two MAX-DOAS instruments and averaged surface NO_2 VMRs obtained from selected air quality monitoring stations. Only data from air quality monitoring stations having a distance of less than 1.5 km from the respective ground projected MAX-DOAS light path were used. The results of this analysis show that highest correlation coefficients (R) with values reaching up to 0.94 are found for the summer season. When applying well-considered filter criterion to remove measurements taken during situations with unfavorable atmospheric visibility, medium to high correlation coefficients (R = 0.6 to 0.89) could also be found for the other seasons. The results of this analysis imply that path-averaged near-surface NO_2 VMRs are comparable in terms of diurnal variability to surface NO_2 VMRs obtained from air quality monitoring stations, but are lower in magnitude by a factor of about 3–5, depending on the season and viewing direction.

The analysis of seasonal cycles of path-averaged near-surface NO_2, HCHO, and CHOCHO VMRs obtained from the lowest viewing directions pointing towards the location of the other instrument shows that highest values show up during different seasons of the year. While monthly averages of NO_2 amounts peak during the winter season, HCHO amounts are highest on average in the warmer summer season. In contrast to the well pronounced NO_2 and HCHO seasonal cycles, less seasonal variability is found for CHOCHO amounts. As CHOCHO values are also high in winter, we argue that this trace gas is more strongly linked to direct anthropogenic emission sources than HCHO.

Seasonally averaged diurnal cycles show that peaks of path-averaged NO_2 and CHOCHO VMRs generally show up in the morning hours, e.g. when wind speeds are comparatively low and mixing-heights are shallow. In addition, a clear difference is observed for these two trace gases when diurnal cycles obtained for weekdays are compared with those obtained for weekends. Both the diurnal variability and the difference between weekdays and weekends are less pronounced for HCHO, again suggesting that HCHO is predominantly produced from the oxidation of biogenic VOCs.

From the analysis of the azimuthal dependence, knowledge about the horizontal distribution of NO_2, HCHO, and CHOCHO amounts is gained. The highest seasonally-averaged path-averaged NO_2 and CHOCHO VMRs obtained from the lowest elevation angles are observed when the telescopes are pointing towards or close to the city center and towards industrial areas. There is one viewing direction for both MAX-DOAS instruments that indicates slightly lower NO_2 and CHOCHO amounts. We argue that these two azimuthal viewing directions cover rather residential and rural areas in northern and western parts of Vienna. While there is a substantial variability of path-averaged HCHO VMRs obtained from the individual azimuthal viewing directions during the summer season, almost no variability is found in winter, at a time where HCHO amounts are comparatively low.

The amounts of NO_2 and CHOCHO as obtained from the lowest viewing directions pointing towards the city center are both affected by wind direction and wind speed. While only a low impact of wind speed on the trace gas amounts is observed when the wind is blowing from the west, transporting rather clean air to Vienna, wind speed seems to be the determining factor when the wind is blowing from the Southeast. Thus, highest NO_2 and CHOCHO amounts over the city center of Vienna are observed under calm wind conditions (<5 km h^{-1}) and when the wind is

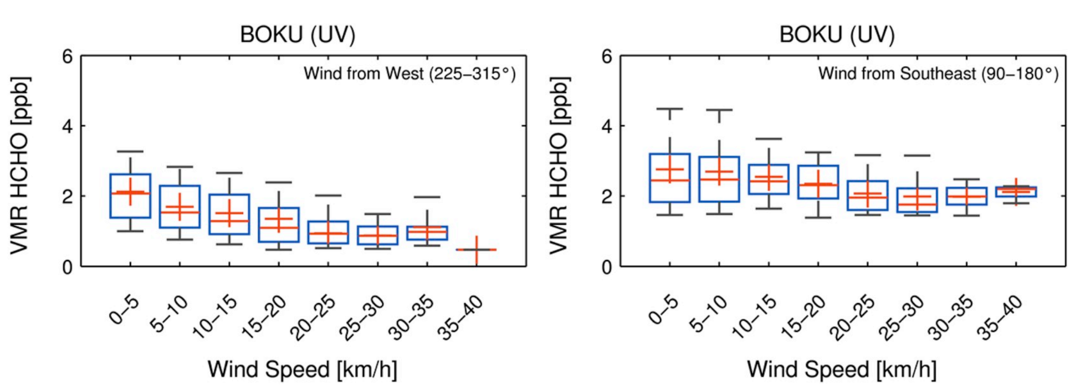

Fig. 15. Same as Fig. 14, but for path-averaged HCHO VMRs obtained from the BOKU instrument (EA = 1°, AA = 137°).

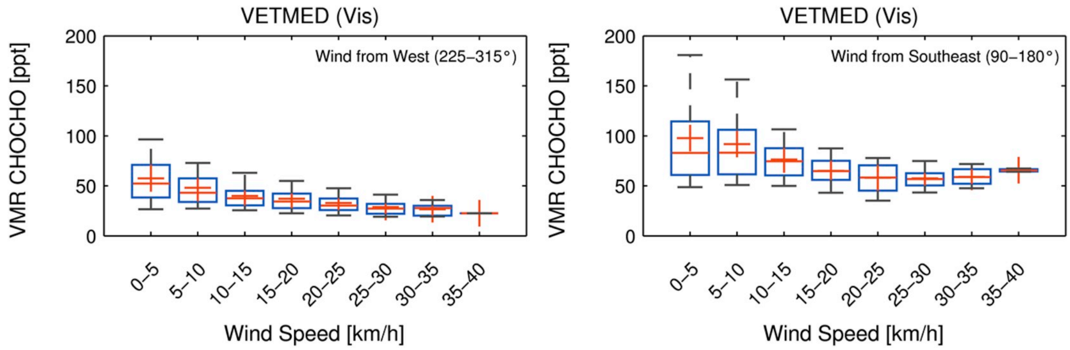

Fig. 16. Same as Fig. 14, but for path-averaged CHOCHO VMRs obtained from the VETMED instrument (EA = 3°, AA = 225°).

blowing from the Southeast. Interestingly, mean HCHO VMRs are highest when southeastern winds range between 5 and 10 km h^{-1}, in addition to cases with calm wind speeds. One reason for this could be transport of HCHO produced from a densely vegetated meadowland and/or from an oil refinery, which are both located about 15 km to the southeast of the city center of Vienna.

In conclusion, the successful set-up and continuous operation of two VINDOBONA MAX-DOAS instruments builds the fundament for research on tropospheric pollution over the urban environment of Vienna. More recently, a third MAX-DOAS was set up on a tower platform at a third location in Vienna, e.g. in the south of the city center. The three instruments make Vienna an attractive site for satellite validation and measurement campaigns.

Author contribution

Stefan F. Schreier and Andreas Richter formulated the overarching goals of the VINDOBONA project. Enno Peters, Stefan F. Schreier, and Mareike Ostendorf assembled the two MAX-DOAS instruments in the laboratory of the IUP-UB. Philipp Weihs and Alois W. Schmalwieser helped in maintaining the two MAX-DOAS instruments in Vienna. Stefan F. Schreier analyzed the data and prepared the manuscript with contributions from all co-authors.

Declaration of competing interest

The authors declare that they have no known competing financial interests or personal relationships that could have appeared to influence the work reported in this paper.

Acknowledgements

This study was funded by the Austrian Science Fund (FWF): I 2296-N29 and the German Research Foundation (DFG): RI 1800/6–1. Many thanks go to (in alphabetical order) Lisa Behrens, Christian Gützer, Sandro Ostwald, Anja Schönhardt, André Seyler, and Folkard Wittrock for their helping hands and technical support during the setup and maintenance of the two MAX-DOAS instruments. We wish to thank "Amt der Niederösterreichischen Landesregierung", "MA22 der Stadt Wien" and "Umweltbundesamt" for making the air quality data freely available. The provision of meteorological data by the Austrian official weather service (ZAMG) is also acknowledged. Finally, we wish to thank Christoph Lotteraner and Martin Piringer (ZAMG) for providing time-series of mixing-height.

Appendix A. Supplementary data

Supplementary data to this article can be found online at https://doi.org/10.1016/j.aeaoa.2019.100059.

References

Alvarado, L.M.A., Richter, A., Vrekoussis, M., Wittrock, F., Hilboll, A., Schreier, S.F., Burrows, J.P., 2014. An improved glyoxal retrieval from OMI measurements. Atmos. Meas. Tech. 7, 4133–4150. https://doi.org/10.5194/amt-7-4133-2014.

Aron, R., 1983. Mixing height – an inconsistent indicator of potential air pollution concentrations. Atmos. Environ. 17, 2193–2197.

Augustyn, R., Bachl, R., Kellner, C., Planck, R., Tizek, H., Jahresbericht, 2018. Luftgütemessungen der Umweltschutzabteilung der Stadt Wien gemäß Immissionsschutzgesetz – Luft. MA22 – 624030/2018, 2018.

Beirle, S., Boersma, K.F., Platt, U., Lawrence, M.G., Wagner, T., 2011. Megacity emissions and lifetimes of nitrogen oxides probed from space. Science 333, 1737–1739.

Burrows, J., Hölzle, E., Goede, A., Visser, H., Fricke, W., 1995. SCIAMACHY – scanning imaging absorption spectrometer for atmospheric chartography. Acta Astronaut. 35, 445–451.

Burrows, J.P., Weber, M., Buchwitz, M., Rozanov, V., Ladstätter-Weißenmayer, A., Richter, A., DeBeek, R., Hoogen, R., Bramstedt, K., Eichmann, K.-U., Eisinger, M., Perner, D., 1999. The global ozone monitoring experiment(GOME): mission concept and first scientific results. J. Atmos. Sci. 56, 151–175.

Burrows, J.P., Platt, U., Borrell, P., 2011. The Remote Sensing of Tropospheric Composition from Space, first ed. Springer, Heidelberg, Germany.

Chan, K., Wiegner, M., Wenig, M., Pöhler, D., 2018. Observations of tropospheric aerosols and NO2 in Hong Kong over 5 years using ground-based MAX-DOAS. Sci. Total Environ. 619–620, 1545–1556. https://doi.org/10.1016/j.scitotenv.2017.10.153.

Chan Miller, C., Gonzalez Abad, G., Wang, H., Liu, X., Kurosu, T., Jacob, D.J., Chance, K., 2014. Glyoxal retrieval from the ozone monitoring instrument. Atmos. Meas. Tech. 7, 3891–3907. https://doi.org/10.5194/amt-7-3891-2014.

Crutzen, P.J., 1979. The role of NO and NO2 in the chemistry of the troposphere and stratosphere. Annu. Rev. Earth Planet Sci. 7, 443–472.

Crutzen, P.J., 1970. The influence of nitrogen oxides on the atmospheric ozone content. Q. J. Roy. Meteor. Soc. 96, 320–325.

De Smedt, I., Stavrakou, T., Müller, J.F., van der A, R., Van Roozendael, M., 2010. Trend detection in satellite observations of formaldehyde tropospheric columns. Geophys. Res. Lett. 37 https://doi.org/10.1029/2010GL044245. L18808.

Delmas, R., Serça, D., Jambert, C., 1997. Global inventory of NOx sources. Nutrient Cycl. Agroecosyst. 48, 51–60.

Dirksen, R.J., Boersma, K.F., Eskes, H., Ionov, D.V., Bucsela, E.J., Levelt, P.F., Kelder, H. M., 2011. Evaluation of stratospheric NO2 retrieved from the Ozone Monitoring Instrument: intercomparison, diurnal cycle and trending. J. Geophys. Res. 116, D08305. https://doi.org/10.1029/2010JD014943.

Finlayson-Pitts, B.J., Pitts, J.N., 2000. Chemistry of the Upper and Lower Atmosphere: Theory, Experiments and Applications. Academic Press, San Diego.

Fleischmann, O.C., Hartmann, M., Burrows, J.P., Orphal, J., 2004. New ultraviolet absorption cross-sections of BrO at atmospheric tempera-tures measured by time-windowing Fourier transform spectroscopy. J. Photochem. Photobiol. A Chem. 168, 117–132. https://doi.org/10.1016/j.jphotochem.2004.03.026. http://www.sciencedirect.com/science/article/pii/S1010603004001522.

Fu, T.-M., Jacob, D.J., Palmer, P.I., Chance, K., Wang, Y.X., Barletta, B., Blake, D.R., Stanton, J.C., Pilling, M.J., 2007. Space-based formaldehyde measurements as constraints on volatile organic compound emissions in east and south Asia and implications for ozone. J. Geophys. Res. 112, D06312 doi:10.29/2006JG007853.

Fu, T.-M., Jacob, D.J., Wittrock, F., Burrows, J.P., Vrekoussis, M., Henze, D.K., 2008. Global budgets of atmospheric glyoxal and methylglyoxal, and implications for formation of secondary organic aerosols. J. Geophys. Res.-Atmos. 113, D15303. https://doi.org/10.1029/2007JD009505.

Gomez, L., Navarro-Comas, M., Puentedura, O., Gonzalez, Y., Cuevas, E., Gil-Ojeda, M., 2014. Long-path averaged mixing ratios of O3 and NO2 in the free troposphere from mountain MAX-DOAS. Atmos. Meas. Tech. 7, 3373–3386. https://doi.org/10.5194/amt-7-3373-2014.

Gratsea, M., Vrekoussis, M., Richter, A., Wittrock, F., Schönhardt, A., Burrows, J., Kazadzis, S., Mihalopoulos, N., Gerasopoulos, E., 2016. Slant Column MAX-DOAS measurements of nitrogen dioxide, formaldehyde, glyoxal and oxygen dimer in the urban environment of Athens. Atmos. Environ. 135, 118–131. https://doi.org/10.1016/j.atmosenv.2016.03.048.

Hendrick, F., Müller, J.-F., Clémer, K., Wang, P., De Mazière, M., Fayt, C., Gielen, C., Hermans, C., Ma, J.Z., Pinardi, G., Stavrakou, T., Vlemmix, T., Van Roozendael, M., 2014. Four years of ground-based MAX-DOAS observations of HONO and NO2 in the Beijing area. Atmos. Chem. Phys. 14, 765–781. https://doi.org/10.5194/acp-14-765-2014.

Hönninger, G., von Friedeburg, C., Platt, U., 2004. Multi axis differential optical absorption spectroscopy (MAX-DOAS). Atmos. Chem. Phys. 4, 231–254. https://doi.org/10.5194/acp-4-231-2004.

Houweling, S., Dentener, F., Lelieveld, J., 1998. The impact of nonmethane hydrocarbon compounds on tropospheric photochemistry. J. Geophys. Res. 103 (D9), 10,673–10,696.

Jang, M., Kamens, R.M., 2001. Characterization of secondary organic aerosol from the photooxidation of toluene in the presence of NOx and 1-propene. Environ. Sci. Technol. 35, 3626–3639.

Kramer, L.J., Leigh, R.J., Remedios, J.J., Monks, P.S., 2008. Comparison of OMI and ground-based in situ and MAX-DOAS measurements of tropospheric nitrogen dioxide in an urban area. J. Geophys. Res. 113, D16S39. https://doi.org/10.1029/2007jd009168.

Kreher, K., Van Roozendael, M., Hendrick, F., Apituley, A., Dimitropoulou, E., Frieß, U., Richter, A., Wagner, T., Abuhassan, N., Ang, L., Anguas, M., Bais, A., Benavent, N., Bösch, T., Bognar, K., Borovski, A., Bruchkouski, I., Cede, A., Chan, K.L., Donner, S., Drosoglou, T., Fayt, C., Finkenzeller, H., Garcia-Nieto, D., Gielen, C., Gómez-Martín, L., Hao, N., Herman, J.R., Hermans, C., Hoque, S., Irie, H., Jin, J., Johnston, P., Khayyam Butt, J., Khokhar, F., Koenig, T.K., Kuhn, J., Kumar, V., Lampel, J., Liu, C., Ma, J., Merlaud, A., Mishra, A.K., Müller, M., Navarro-Comas, M., Ostendorf, M., Pazmino, A., Peters, E., Pinardi, G., Pinharanda, M., Piters, A., Platt, U., Postylyakov, O., Prados-Roman, C., Puentedura, O., Querel, R., Saiz-Lopez, A., Schönhardt, A., Schreier, S.F., Seyler, A., Sinha, V., Spinei, E., Strong, K., Tack, F., Tian, X., Tiefengraber, M., Tirpitz, J.-L., van Gent, J., Volkamer, R., Vrekoussis, M., Wang, S., Wang, Z., Wenig, M., Wittrock, F., Xie, P.H., Xu, J., Yela, M., Zhang, C., Zhao, X., 2019. Intercomparison of NO2, O4, O3 and HCHO slant column measurements by MAX-DOAS and zenith-sky UV-Visible spectrometers during the CINDI-2 campaign. Atmos. Meas. Tech. Discuss. https://doi.org/10.5194/amt-2019-157 submitted for publication.

Kurucz, R.L., Furenhild, I., Brault, J., Testermann, L., 1984. Solar Flux Atlas from 296 to 1300 nm, National Solar Observatory Atlas No. 1. June.

Lerot, C., Stavrakou, T., De Smedt, I., Müller, J.-F., Van Roozendael, M., 2010. Glyoxal vertical columns from GOME-2 backscattered light measurements and comparisons with a global model. Atmos. Chem. Phys. 10, 12059–12072. https://doi.org/10.5194/acp-10-12059-2010.

Lotteraner, C., Piringer, M., 2016. Mixing-height time series from operational ceilometer aerosol-layer heights. Bound.-Lay. Meteorol. 161, 265–287. https://doi.org/10.1007/s10546-016-0169-2.

Ma, J.Z., Beirle, S., Jin, J.L., Shaiganfar, R., Yan, P., Wagner, T., 2013. Tropospheric NO2 vertical column densities over Beijing: results of the first three years of ground-based MAX-DOAS measurements (2008–2011) and satellite validation. Atmos. Chem. Phys. 13, 1547–1567. https://doi.org/10.5194/acp-13-1547-2013.

Meller, R., Moortgat, G.K., 2000. Temperature dependence of the absorption cross sections of formaldehyde between 223 and 323 K in the415wavelength range 225–375 nm. J. Geophys. Res.: Atmosphere 105, 7089–7101. https://doi.org/10.1029/1999JD901074. http://onlinelibrary.wiley.com/doi/10.1029/1999JD901074/abstract.

Noxon, J.F., 1975. Nitrogen dioxide in the stratosphere and troposphere measured by ground based absorption spectroscopy. Science 189, 547–549.

Palmer, P.I., Jacob, D.J., Fiore, A.M., Martin, R.V., Chance, K., Kurosu, T.P., 2003. Mapping isoprene emissions over North America using formaldehyde column observations from space. J. Geophys. Res.-Atmos. 108 (D6), 4180. https://doi.org/10.1029/2002jd002153.

Parrish, D.D., Ryerson, T.B., Mellqvist, J., Johansson, J., Fried, A., Richter, D., Walega, J. G., Washenfelder, R.A., de Gouw, J.A., Peischl, J., Aikin, K.C., McKeen, S.A., Frost, G. J., Fehsenfeld, F.C., Herndon, S.C., 2012. Primary and secondary sources of formaldehyde in urban atmospheres: houston Texas region. Atmos. Chem. Phys. 12, 3273–3288. https://doi.org/10.5194/acp-12-3273-2012.

Perner, D., Platt, U., 1979. Detection of nitrous acid in the atmosphere by differential optical absorption. Geophys. Res. Lett. 6, 917–920.

Platt, U., Stutz, J., 2008. Differential Optical Absorption Spectroscopy. Physics of Earth and Space Environments. Springer, Berlin.

Richter, A., 1997. Absorptionsspektroskopische Messungen stratosphärischer Spurengase über Bremen, 53°N, PhD thesis. University of Bremen.

Richter, A., Eisinger, M., Ladstätter-Weißenmayer, A., Burrows, J.P., 1999. DOAS zenith sky observations: 2. Seasonal variation of BrO over Bremen (53°N) 1994-1995. J. Atmos. Chem. 32, 83–99.

Schreier, S.F., Richter, A., Wittrock, F., Burrows, J.P., 2016. Estimates of free-tropospheric NO2 and HCHO mixing ratios derived from high-altitude mountain MAX-DOAS observations at midlatitudes and in the tropics. Atmos. Chem. Phys. 16, 2803–2817. https://doi.org/10.5194/acp-16-2803-2016.

Rothmann, L.S., Barbe, A., Benner, D.C., Brown, L.R., Camy-Peyret, C., Carleer, M.R., Chance, K., Clerbaux, C., Dana, V., Devi, V.M., Fayt, A., Flaud, J.-M., Gamache, R.R., Goldman, A., Jacquemart, D., Jucks, K.W., Lafferty, W.J., Mandin, J.-Y., Massie, S.T., Nemtchinov, V., Newnham, D.A., Perrin, A., Rinsland, C.P., Schroeder, J., Smith, K. M., Smith, M.A.H., Tang, K., Toth, R.A., Auwera, J.V., Varanasi, P., Yoshino, K., 2003. The HITRAN molecular spectroscopic database: edition of 2000 including updates through 2001. J. Quant. Spectrosc. Radiat. Transf. 82 (5–44).

Schreier, S.F., Richter, A., Burrows, J.P., 2019. Near-surface and path-averaged mixing ratios of NO2 derived from car DOAS zenith-sky and tower DOAS off-axis measurements in Vienna: a case study. Atmos. Chem. Phys. 19, 5853–5879. https://doi.org/10.5194/acp-19-5853-2019.

Serdyuchenko, A., Gorshelev, V., Weber, M., Chehade, W., Burrows, J.P., 2014. High spectral resolution ozone absorption cross-sections – Part 2: temperature dependence. Atmos. Meas. Tech. 7, 625–636. https://doi.org/10.5194/amt-7-625-2014.

Seyler, A., Wittrock, F., Kattner, L., Mathieu-Üffing, B., Peters, E., Richter, A., Schmolke, S., Burrows, J.P., 2017. Monitoring shipping emissions in the German Bight using MAX-DOAS measurements. Atmos. Chem. Phys. 17, 10997–11023. https://doi.org/10.5194/acp-17-10997-2017.

Singh, H., Chen, Y., Staudt, A., Jacob, D., Blake, D., Heikes, B., Snow, J., 2001. Evidence from the Pacific troposphere for large global sources of oxygenated organic compounds. Nature 410, 1078–1081.

Sinreich, R., Merten, A., Molina, L., Volkamer, R., 2013. Parameterizing radiative transfer to convert MAX-DOAS dSCDs into near-surface box-averaged mixing ratios. Atmos. Meas. Tech. 6, 1521–1532. https://doi.org/10.5194/amt-6-1521-2013.

Solomon, S., Schmeltekopf, A.L., Sanders, R.W., 1987. On the interpretation of zenith sky absorption measurements. J. Geophys. Res. 92, 8311–8319.

Spangl, W., Nagl, C., 2017. Jahresbericht der Luftgütemessungen in Österreich 2016, REPORT REP-0605. Umweltbundesamt GmbH, Wien.

Stavrakou, T., Müller, J.-F., De Smedt, I., Van Roozendael, M., Kanakidou, M., Vrekoussis, M., Wittrock, F., Richter, A., Burrows, J.P., 2009. The continental source of glyoxal estimated by the synergistic use of spaceborne measurements and inverse modelling. Atmos. Chem. Phys. 9, 8431–8446. https://doi.org/10.5194/acp-9-8431-2009.

Thalman, R., Volkamer, R., 2013. Temperature dependent absorption cross-sections of O2-O2 collision pairs between 340 and 630 nm and at atmospherically relevant pressure. Phys. Chem. Chem. Phys. 15, 15371–15381. https://doi.org/10.1039/c3cp50968k.

Vandaele, A.C., Hermans, C., Simon, P.C., Roozendael, M.V., Guilmot, J.M., Carleer, M., Colin, R., 1996. Fourier transform measurement of NO2 absorption cross-section in the visible range at room temperature. J. Atmos. Chem. 25, 289–305.

Vlemmix, T., Eskes, H.J., Piters, A.J.M., Schaap, M., Sauter, F.J., Kelder, H., Levelt, P.F., 2015. MAX-DOAS tropospheric nitrogen dioxide column measurements compared with the Lotos-Euros air quality model. Atmos. Chem. Phys. 15, 1313–1330. https://doi.org/10.5194/acp-15-1313-2015.

Volkamer, R., Molina, L.T., Molina, M.J., Shirley, T., Brune, W.H., 2005. DOAS measurement of glyoxal as an indicator for fast VOC chemistry in urban air. Geophys. Res. Lett. 32 (8), L08806. https://doi.org/10.1029/2005GL022616.

Volkamer, R., Spietz, P., Burrows, J., Platt, U., 2005. High-resolution absorption cross-section of glyoxal in the UV–vis and IR spectral ranges. J. Photochem. Photobiol. A Chem. 172, 35–46. https://doi.org/10.1016/j.jphotochem.2004.11.011. http://www.sciencedirect.com/science/article/pii/S1010603004005143.

Vrekoussis, M., Wittrock, F., Richter, A., Burrows, J.P., 2009. Temporal and spatial variability of glyoxal as observed from space. Atmos. Chem. Phys. 9, 4485–4504. https://doi.org/10.5194/acp-9-4485-2009.

Wagner, T., Dix, B., Friedeburg, C.V., Frieß, U., Sanghavi, S., Sinreich, R., Platt, U., 2004. MAX-DOAS O4 measurements: a new technique to derive information on atmospheric aerosols - principles and information content. J. Geophys. Res. D Atmos. 109, 1–19.

Wagner, T., Beirle, S., Brauers, T., Deutschmann, T., Frieß, U., Hak, C., Halla, J.D., Heue, K.P., Junkermann, W., Li, X., Platt, U., Pundt-Gruber, I., 2011. Inversion of tropospheric profiles of aerosol extinction and HCHO and NO2 mixing ratios from MAX-DOAS observations in Milano during the summer of 2003 and comparison with independent data sets. Atmos. Meas. Tech. 4, 2685–2715. https://doi.org/10.5194/amt-4-2685-2011.

Wang, Y., Lampel, J., Xie, P., Beirle, S., Li, A., Wu, D., Wagner, T., 2017. Ground-based MAX-DOAS observations of tropospheric aerosols, NO2, SO2 and HCHO in Wuxi, China, from 2011 to 2014. Atmos. Chem. Phys. 17, 2189–2215. https://doi.org/10.5194/acp-17-2189-2017.

Wang, Y., Li, A., Xie, P.H., Wagner, T., Chen, H., Liu, W.Q., Liu, J.G., 2014. A rapid method to derive horizontal distributions of trace gases and aerosols near the surface using multi-axis differential optical absorption spectroscopy. Atmos. Meas. Tech. 7, 1663–1680. https://doi.org/10.5194/amt-7-1663-2014.

Wittrock, F., Müller, R., Richter, A., Bovensmann, H., Burrows, J.P., 2000. Measurements of iodine monoxide (IO) above spitsbergen. Geophys. Res. Lett. 27, 1471–1474.

Wittrock, F., Oetjen, H., Richter, A., Fietkau, S., Medeke, T., Rozanov, A., Burrows, J.P., 2004. MAX-DOAS measurements of atmospheric trace gases in Ny-Ålesund – radiative transfer studies and their application. Atmos. Chem. Phys. 4, 955–966. https://doi.org/10.5194/acp-4-955-2004.

Wittrock, F., Richter, A., Oetjen, H., Burrows, J.P., Kanakidou, M., Myriokefalitakis, S., Volkamer, R., Beirle, S., Platt, U., Wagner, T., 2006. Simultaneous global observations of glyoxal and formaldehyde from space. Geophys. Res. Lett. 33, L16804. https://doi.org/10.1029/2006GL026310.

Xing, C., Liu, C., Wang, S., Chan, K.L., Gao, Y., Huang, X., Su, W., Zhang, C., Dong, Y., Fan, G., Zhang, T., Chen, Z., Hu, Q., Su, H., Xie, Z., Liu, J., 2017. Observations of the vertical distributions of summertime atmospheric pollutants and the corresponding ozone production in Shanghai, China. Atmos. Chem. Phys. 17, 14275–14289. https://doi.org/10.5194/acp-17-14275-2017.